

Solvation, relaxation, and geminate recombination of electrons generated by two 200 nm photon ionization of liquid H₂O and D₂O.¹

Rui Lian, Robert A. Crowell,^{*} and Ilya A. Shkrob.

^aChemistry Division, Argonne National Laboratory, Argonne, IL 60439

The submitted manuscript has been created by the University of Chicago as Operator of Argonne National Laboratory ("Argonne") under Contract No. W-31-109-ENG-38 with the U. S. Department of Energy. The U. S. Government retains for itself, and others acting on its behalf, a paid-up, nonexclusive, irrevocable worldwide license in said article to reproduce, prepare derivative works, distribute copies to the public, and perform publicly and display publicly, by or on behalf of the Government.

Abstract

Temporal evolution of transient absorption spectra for pre-solvated electron generated by biphotonic (200 nm) ionization of liquid H₂O and D₂O has been studied on femto- and pico- second time scales. These spectra were obtained in the intervals of 50 nm between 0.5 and 1.7 μ m. Two distinctive regimes of the spectral evolution were observed. In both of these regimes, the spectral profile changes considerably with delay time. The "continuous blue shift" and "temperature jump" models are not supported by our data. For $t < 1$ ps, two new features (the 1.15 μ m band and 1.4 μ m shoulder) were observed for the electron in the spectral region where O-H overtones appear in the spectra of light water. These two features were not observed for the electron in D₂O. Vibronic coupling to the modes of water molecules lining the solvation cavity is a possible origin of these features. On the sub-picosecond time scale, the absorption band of solvated electron progressively shifts to the blue. At later delay times ($t > 1$ ps), the position of the band maximum is "locked", but the spectral profile continues to change by narrowing on the red side and broadening on the blue side; the oscillator strength is constant within 10%. The time constant of this narrowing is ca. 0.56 ps for H₂O and 0.64 ps for D₂O, respectively. Vibrational relaxation and time-dependent decrease in the size and

anisotropy of the solvation cavity are suggested as possible causes for the observed spectral transformations in both of these regimes.

The geminate recombination kinetics for hydrated electrons generated by absorption of two 200 nm quanta (12.4 eV total energy) in light and heavy water are almost identical. The kinetic analysis suggests that the average separation between the electron and its geminate partners (ca. 2.4 nm for light water) in D₂O is 13% narrower than in H₂O, which suggests that autoionization of water competes with direct ionization even at this high photoexcitation energy.

¹ Work performed under the auspices of the Office of Science, Division of Chemical Science, US-DOE under contract number W-31-109-ENG-38.

* To whom correspondence should be addressed: *Tel* 630-252-8089, *FAX* 630-2524993, *e-mail*: rob_crowell@anl.gov.

1. Introduction.

Although ultrafast dynamics of the excess electron in liquid water have been extensively studied over the last two decades, many questions concerning the mechanism of thermalization, localization, and solvation of this electron still remain. [1] Using femtosecond pump-probe transient absorbance (TA) laser spectroscopy, short-lived precursors of the thermalized, hydrated electrons (which in the following will be collectively called "pre-solvated" electrons) have been observed on sub-picosecond time scale. [2] Common means of generating these pre-solvated electrons include multiphoton ionization of neat water [3], photoionization of solutes and charge-transfer-to-solvent (CTTS) photoexcitation of aqueous anions, [4] and photoexcitation of hydrated electrons. [5] The initial studies [6] were limited to the observation of the TA signal for a few strategically chosen probe wavelengths in the visible and near-IR. Recently, the observation range has been expanded into the UV (out to 200 nm) [7] and mid-IR (out to 3 μm). [8] The latter studies by Laubereau and co-workers seem to suggest the existence of two IR-absorbing precursors of the hydrated electron, e_{aq}^- . One of these species has a broad absorption band centered at 1.6 μm (suggesting a localized state in a shallow trap [9]), while another species has a featureless spectrum that resembles that of a free (extended state) conduction band electron in semiconductor solids [10] (it also looks similar to the long-lived, IR-absorbing electron in low-temperature ice [11]). While the existence of the short-lived IR-absorbing species has been hinted at by the pioneering study of Migus et al., [12] subsequent work on electron solvation in photoionization of water favored the so-called "continuous shift" model in which the existence of these IR-absorbing species ("wet" electrons) is not strictly required. In the latter model, the absorption profile $S(E, t)$ of the pre-solvated electron is postulated to shift to the blue as a whole during the solvation, without changing its shape.

In a more recent variant of this model suggested by Keiding and coworkers [13] (which is referred to in the following as the "temperature jump" model), the thermalization is regarded as "cooling" of water around the solvation cavity in which the absorption spectrum of the electron at any time during the thermalization process is identical to the spectrum of hydrated electron in the state of equilibrium with the solvent

at some higher temperature. In this model, the electron thermalization is viewed as a succession of quasi-equilibrium states that are fully characterized by the time evolution of the local temperature. [1] This model, like the "continuous shift" model considered above is purely phenomenological: no explanation is given on the theoretical grounds, as to why such a picture of the electron solvation might be correct. The recent theoretical study of Borgis and coworkers, [2] for example, strongly suggests that the temperature dependence of the e_{aq}^- spectrum is determined primarily by a bulk property of water: namely, its density; increasing the temperature is just a way of changing this density. Such a property is not local, as tacitly assumed in the "temperature jump" model. Since the shape of the absorption spectrum of e_{aq}^- weakly depends on the water temperature (see Appendix A in the Supplement), whereas the position of the absorption maximum is strongly temperature dependent, from the standpoint of data analysis, the "temperature jump" model of Keiding and coworkers [3] is nearly identical to the "continuous shift" model. Despite their current popularity, the "continuous shift" and "temperature jump" models of electron solvation are inadequately supported:

First, in many ultrafast studies, the TA spectra were too sparsely sampled: the TA kinetics were obtained for just 4-to-10 wavelengths of the probe light. This sparse sampling makes it impossible to verify the central tenet of the "continuous shift" model, *viz.* the constancy of the spectral profile during the thermalization process. Typically, [4] this constancy was *postulated* rather than observed: For a given delay time t of the probe pulse, the (sparse) TA spectrum was fit by a constant-profile template using the least squares optimization. As a result, the experimental spectrum is characterized by a single parameter, $E_{\max}(t)$, the photon energy corresponding to the absorption maximum. Naturally, this procedure tells little about the robustness of the template used to fit the experimental spectrum since any deviation from the prescribed shape is regarded as statistical "noise". Worse, the exact location of the maximum strongly depends on the template used to fit the data, inasmuch as the electron spectra are flat at the top, broad, and featureless, so that $E_{\max}(t)$ is determined, implicitly or explicitly, by the extrapolation of the data in the spectral wings towards the center, where the TA signal is maximum. If the profile of the sparsely-sampled TA spectra were time-dependent (as suggested by our results), this approach would yield grossly incorrect results.

Second, the TA studies in which the spectral sampling was sufficiently dense (at least 10-15 wavelengths of the probe light across the spectrum) *did not* fully support the "continuous shift" model. [1] E.g., the benchmark studies by Gauduel and coworkers [1] and Jay-Gerin and coworkers [1] on electron dynamics in H₂O and D₂O, respectively, indicated that the "continuous shift" alone cannot account for the observed spectral evolution. In the latter study, an additional long-lived (> 2 ps) species with a spectral band centered at 1.1-1.3 μ m was postulated to explain the evolution of the TA spectrum for $\lambda > 0.9 \mu$ m. Subsequent pump-probe studies failed to verify the existence of such a long-lived species. Part of the problem was that the spectral evolution of spectrum in the near-IR was obtained using TA kinetics that exhibited poor signal-to-noise (S/N) ratio (3:1 to 10:1). The authors [1] conceded that more TA studies with dense sampling of the TA kinetics across a wider spectral region and better-quality kinetic data would be needed to characterize the spectral evolution and establish the validity of the "continuous shift" model. The present study implements such a program.

Third, it is now understood that the electrons generated in different photoprocesses have somewhat different thermalization [1] and recombination [1] dynamics. Specifically, in photoionization of neat water, different excitation mechanisms operate for photons of different energy. [1] Two- or three-photon excitation at the lower photon energy (so that the total excitation energy < 9 eV) produces the electrons that are, on average, just 0.9-1 nm away from their parent hole, whereas at higher total photon energy (> 11 eV), the photoelectrons are at least 2-3 nm away. It is believed that for high-energy photoexcitation, the electrons are ejected directly into the conduction band of the solvent; [1] at lower energy, the photoionization involves concerted proton and electron transfers, perhaps to pre-existing traps. [1] In the intermediate regime, autoionization of water is thought to compete with these two photoprocesses. [1] The studies with the densest spectral sampling were carried out in these low-energy and intermediate regimes. [1] Due to the short separation distances between the geminate partners, some electrons decayed during the first few picoseconds when their thermalization and solvation had occurred. This decay had to be taken into account, by extrapolation of the picosecond dynamics to short delay times. Such a procedure implies that the pre-solvated electron follows the same recombination dynamics as fully thermalized, hydrated electron, which

may not be correct. E.g., recent simulations of spectral evolution for electrons generated in the iodide CTTS (carried out using the “continuous shift” model) by Bradford and co-workers suggested significantly faster decay rate for the short-lived pre-solvated species.

□

In the present study, femto- and pico- second TA kinetics were obtained for the electron generated in high-energy ionization photoprocess (12.4 eV total energy); in this regime, the geminate recombination on the picosecond time scale is unimportant (sections 3.1 and 4.1). Short 200 nm (300 fs fwhm) laser pulses were used to photoionize room temperature H₂O and D₂O via biphotonic excitation. A set of TA kinetics obtained with time resolution of 50 fs was sampled out to 5-30 ps in steps of 50 nm from 0.5 to 1.4 μ m (to 1.7 μ m for D₂O). Throughout this entire spectral range, the S/N ratio for the individual kinetics was better than 50:1.

Our results suggest that the “continuous shift” model does not fully account for the spectral evolution occurring during the electron solvation/thermalization in light and heavy water. Neither the shape of the TA spectra is constant, nor the thermalization dynamics can be reduced to the shift of the band maximum. For $t > 1$ ps, the electron spectrum exhibits progressive line narrowing in the red (concomitant with the line broadening in the blue). This change continues well after the spectral shift is completed; it probably results from the vibrational relaxation of water molecules around the “hot” ground-state electron. Furthermore, for electron in H₂O, new features were observed in the near-IR on sub-picosecond time scale. One of these features might have been observed previously by Laenen et al. □ in H₂O and D₂O (a band centered at 1.6 μ m), another, with a band centered at 1.15 μ m, might be the tentative IR-absorbing species predicted by Jay-Gerin and coworkers □. No evidence of these two features has been found in *heavy* water, in a striking contradiction to the results of Laenen et al. □. It appears that these absorption bands do not originate from a purely electronic transition. Rather, these bands seem to involve *vibrations* of the water molecules.

We forewarn the reader that no specific model that accounts for these observations is given in this paper. Many models of electron solvation and relaxation, at all levels of theory, have been suggested. Given the limited success that these theories met in explanation of experimental observations, offering yet another such model seems

injudicious. Rather, we focus on the spectral features themselves and what can be glimpsed from these features without the benefit of theoretical insight. Such an insight is certainly needed, but it is beyond the scope of this study.

2. Experimental.

Materials. Deionized water with conductivity < 2 nS/cm was used in all experiments with H₂O. N₂-saturated 1 L sample was circulated using a gear pump trough a jet nozzle. A 500 mL sample of heavy water (99 atom %, Aldrich) was used in all experiments with D₂O. No change in the kinetics was observed after continuous photolysis of this sample. The details of the flow system are given elsewhere. [1]

Ultrafast laser spectroscopy. The pico- and femto- second TA measurements were carried out using a 1 kHz Ti:sapphire setup details of which are given in refs. [2]. This setup provided 60 fs FWHM, 3 mJ light pulses centered at 800 nm. One part of the beam was used to generate probe pulses while the other part was used to generate the 200 nm (fourth harmonic) pump pulses. Up to 20 μ J of the 200 nm light was produced this way (300-350 fs FWHM pulse). The pump and probe beams were perpendicularly polarized and overlapped at the surface of a 90 μ m thick high-speed water jet at 5°. No change of the TA kinetics with the polarization of the probe light was observed.

A white light supercontinuum was generated by focussing the 800 nm fundamental on a 1 mm thick sapphire disk; the probe light was selected using a set of 10 nm FWHM interference filters (Corion). For two wavelengths, 1.6 and 1.7 μ m (used in the studies of electron in D₂O), the intensity of the probe light was weak and 30 nm FWHM bandpass filters were used instead (which resulted in a shorter probe pulse). Appropriate cutoff glass filters were used to block stray 200, 400, and 800 nm light. For measurements in the near-IR, 0° dielectric mirrors for 800 nm light were inserted in the path of the probe beam to reduce the leakage of the fundamental. Fast Si photodiodes (FND100Q from EG&G) biased at -90 V were used for detection of the $\lambda < 1.3$ μ m light, fast Ge photodiodes (GMP566 from GPD Optoelectronics Corp.) biased at -9 V were used for detection of $\lambda > 1.2$ μ m. Due to the considerable dark current for the Ge

photodiodes, the load resistance was relatively low, ca. $0.2\text{ M}\Omega$ vs. $6\text{ M}\Omega$ for Si photodiode, which lead to lower sensitivity. The vertical bars in the figures represent 95% confidence limits for each data point. The pump power, before and after the sample, was monitored using a thermopile power meter (Ophir Optronics model 2A-SH).

To study geminate recombination of hydrated electrons, 150-200 delay time points acquired on a quasi-logarithmic grid were used to obtain the decay kinetics of the electron out to 600 ps. To study the thermalization dynamics of the electron, the delay time was increased in steps of 50 fs to 5-7 ps and steps of 300 fs to 25 ps. The kinetic origin (i.e., zero delay time t) and the $1/e$ width τ_p of the 200 nm excitation pulse convoluted with the probe pulse were determined by following the TA signal from a $1.4\text{ }\mu\text{m}$ thick amorphous Si:H alloy film on suprasil substrate. This sample was mounted on a translation stage and positioned into the plane of the jet surface. The typical photoresponse of this semiconductor sample following 200 nm photoexcitation are shown in Fig. 1S (hereafter, the index "S" indicates that the material is placed in the Supporting Information available electronically from the journal). The instantaneous increase in the TA signal near the kinetic origin is from the generation of free electron carriers in the Si:H sample, the slower decay kinetics are due to the thermalization, trapping, and recombination of these photocarriers. Deconvolution of these TA signals (represented as a Gaussian pulse convoluted with biexponential decay to a plateau) gives the "pulse width" τ_p (characteristic of the response function of the setup). Due to the considerable chirp in the 200 nm pump pulse (introduced by harmonic-generating BBO crystals and focussing optics), τ_p was 190-290 fs, depending on the optimization of the compressor and the probe wavelength. The latter dependence is due to the wavelength-dependent chirp in the white light continuum and group velocity mismatch (GVM) in the water sample (traceable to the difference in the speed of light for the pump and probe pulses). The shortest τ_p were obtained near the 800 nm fundamental, the longest - in the near IR. This variation and the resulting uncertainty in the time origin made it difficult to obtain good-quality electron spectra for $t < 500$ fs. For $\lambda < 700$ nm, the TA traces exhibit a sharp "spike" at the time origin (see Fig. 2(a) in section 3.2) whose time profile follows the response function of the detection system. This TA signal in the visible has been

observed by other workers [1] and originates from nonlinear absorbance of the excitation and probe light in the sample. It can be used to juxtapose the corresponding kinetics in time without using the reference Si:H sample. Since the photoexcitation wavelength of 200 nm is right at the onset of one-photon water ionization (the quantum yield of this ionization is ca. 1.6×10^{-2} at 193 nm [2]), this artifact may be present even when red and near-IR light is used to probe the electron dynamics (section 3.3).

The kinetic traces given below were obtained using a 1-5 μJ pump pulse focussed, using a thin MgF_2 lens, to a round spot of 300 μm FWHM; the probe beam was typically 50-60 μm FWHM. Radial profiles of these beams at the jet surface were obtained by scanning of a 10 μm pinhole across the beam. The typical TA signal (ΔOD_λ , where λ is the wavelength of the probe light in nanometers) at the maximum was 10-to-60 mOD. Fig. 2S(a) shows the TA signal $\Delta OD_{800}(t)$ obtained at the delay time $t=10$ ps plotted as a function of 200 nm power, for a tightly focussed UV beam (double logarithmic plot). At this delay time, the thermalization is complete and the TA signal is from the hydrated electron, e_{aq}^- . The initial slope of this plot (solid line in Fig. 2S(a)) is close to 1.84 ± 0.07 , indicating *biphotonic* ionization of water by the 200 nm light. At high power, this slope decreases to 1-1.5 due to nonuniform absorbance of the 200 nm light by the sample. [1] When the photoinduced TA signal reaches 0.5-1, the sub-nanosecond kinetics plotted on the logarithmic time scale show the characteristic bend down typical of the bimolecular cross recombination in the sample bulk (compare traces (i) and (ii) in Fig. 2S(b)). [1] These TA kinetics are power-dependent and their time profiles are different from the profile of *geminant* recombination kinetics obtained in the low-power regime. In the latter regime, normalized TA kinetics are independent of the 200 nm light power (Figs. 1 and 2S). Only the latter type kinetics are considered in the rest of this paper.

Reconstruction of the electron spectrum. Time-dependent TA spectra $S(\lambda, t)$ given below were obtained from the TA kinetics using the following approach: [1] The kinetics (obtained independently for each probe wavelength λ) were normalized by the average of the TA signal at $t=5-10$ ps. At this delay time, the $\Delta OD_\lambda(t)$ kinetics reach a plateau: the thermalization phase is complete yet the electron decay due to geminate recombination is

still negligible (see [section 3.1](#)). These normalized kinetics were then weighted by the spectrum $S(\lambda)$ of the thermalized (hydrated electron) to obtain time-dependent spectrum $S(\lambda,t)$ of the pre-solvated electron:

$$S(\lambda,t) = S(\lambda) \Delta OD_\lambda(t) / \Delta OD_\lambda(t = 5 - 10 \text{ ps}) \quad (1)$$

In the near-IR, where e_{aq}^- absorbs poorly, the use of this procedure requires more comment (see also [Appendix A](#) and [Figs. 3S to 6S](#) in the Supplement).

First, since the TA signal from the hydrated electron at $t=5-10$ ps becomes very small relative to the "spike" from the pre-solvated electron ([Figs. 2, 3, and 4](#)), even a small error of a few per cent in the scaling factor $S(\lambda)$ in eq. (1) has a large effect on the extrapolated $S(\lambda,t)$ signal at short delay time. Thus, a high-quality near-IR spectrum of e_{aq}^- in light and heavy water was needed. To this end, a separate flash photolysis study was carried out to obtain a spectrum of e_{aq}^- in H_2O ($\lambda=0.4-1.4 \text{ } \mu\text{m}$) and D_2O ($\lambda=0.4-1.7 \text{ } \mu\text{m}$) ([Appendix A](#)). Second, one should be aware that the weak, long-lived TA signal observed at $t>5$ ps might not be related to e_{aq}^- since the solvent itself weakly absorbs in the near-IR (where overtones of the O-H stretch appear). Specifically, a long-lived thermal signal from laser-heated water could change the transmittance of the probe light. To address such a possibility, 1 M HClO_4 was added to H_2O (hydronium ion scavenges e_{aq}^- with rate constant of $2.3 \times 10^{10} \text{ M}^{-1} \text{ s}^{-1}$). [\[\]](#) This scavenging removed most of the TA signal in the first 300 ps. By comparing the long-term kinetic traces obtained at different wavelengths, we were able to demonstrate that at least 90-95% of the TA signal at 1.1-1.3 μm was from e_{aq}^- ([Fig 7S](#)). However, for $\lambda>1.3 \text{ } \mu\text{m}$, the long-lived TA signal was too weak to obtain good-quality decay kinetics on sub-nanosecond time scale. Thus, we cannot presently confirm that *all* of the long-lived TA signal in the near-IR is due to the absorbance from e_{aq}^- . This uncertainty introduces ambiguity in the reconstruction of the near-IR spectra using eq. (1). We will return to this point in [section 3.3](#).

Third, it is nearly impossible to retain the same characteristics of the probe light (such as its pulse width, chirp, and GVM) across the entire spectral region of interest. For

this reason, obtaining reliable TA spectra $S(\lambda, t)$ using eq. (1) for delay times $t < 500$ fs is impossible without (i) making specific assumptions about these pulse characteristics and (ii) using *ad hoc* kinetic schemes for spectrum modeling (as done, for example, in refs. [1]). Since these kinetic schemes are not unique, the robustness of such an analysis is impossible to gauge. Our philosophy was to analyze the data with as few *ad hoc* assumptions as possible, and for this reason we focus on the evolution of the TA spectra between 0.5 and 3 ps after the photoionization.

3. Results.

3.1. Long-term kinetics ($t > 5$ ps).

Typical geminate recombination kinetics of e_{aq}^- on sub-nanosecond time scale (for $\lambda=0.8$ μm) are shown in Fig. 1. Very similar kinetics for $t > 5$ ps were observed at other probe wavelengths, including $\lambda=266$ nm at which both e_{aq}^- and OH radical absorb light (the 266 nm light was obtained by third harmonic generation). [1] Fig. 1 shows the comparison between the normalized recombination kinetics of e_{aq}^- in H_2O and D_2O for $t < 0.6$ ns; these two traces are identical within the confidence limits of our measurement. Using the IRT model of Pimblott and coworkers commonly used to simulate the dynamics of water spurs, [1] the decay kinetics of e_{aq}^- for a trial distribution $4\pi r^2 P(r)$ of the initial thermalization distances of the electron can be obtained. Typically, the r^2 -Gaussian distribution, $P(r) \propto \exp(-r^2/2\sigma_G^2)$, has been used for such simulations. [1] Since the diffusion coefficients and recombination constants for light and heavy water are different (see Table 1S in the Supplement), different recombination kinetics are expected to be observed in H_2O and D_2O for the same distribution $P(r)$. Conversely, identical recombination kinetics imply different initial distributions $P(r)$. Fitting the kinetics by the IRT model equations (see ref. [1] and caption to Fig. 1 for the parameters and details of the simulation) yields $\sigma_G=2.4$ nm for H_2O and $\sigma_G=2.1$ nm for D_2O : *the distribution in the heavy water is narrower than in the light water*. This result is discussed in section 4.1. Due to the large width of the initial distribution, the electron decay by geminate

recombination is negligible within the first 10 ps. Thus, the spectral evolution observed within the first 3 ps is driven by the solvation dynamics of the electron alone.

3.2. Short-term kinetics ($t < 5$ ps).

Typical TA kinetics observed for pre-solvated electron following two 200 nm photon ionization of light water are shown in Figs. 2, 3, and 4. The complete set of digitized kinetic traces is given in the Supporting Information (see Appendix B for instructions). Most of the trends observed in these kinetic traces have already been seen by others. For $\lambda > 0.8$ μm , the TA signal rapidly increases within the duration of the 200 nm pulse and then slowly decreases to a plateau (Figs. 2(b), 3(b), and 4(a)). The ratio of the maximum TA signal to the signal attained at $t = 5$ ps increases with the increasing probe wavelength λ (e.g., Fig. 4). For D₂O, this ratio increases from ca. 5:1 at 1.1 μm to ca. 10:1 at 1.25 μm to ca. 30:1 at 1.4 μm to ca. 50:1 at 1.6 μm . As the plateau absorbance becomes relatively smaller with the increasing λ , the decay kinetics become progressively faster (e.g., compare the 0.85 and 1.5 μm traces in Figs. 3(a) and 4(a), respectively). In the visible ($\lambda = 0.5$ -0.75 μm), the increase in the TA signal is relatively slow (taking the first 2 ps after the ionization, Figs. 2(a) and 3(a)) and the changes in the kinetic profiles with the wavelength are less pronounced than in the near-IR.

Qualitatively, these trends can be explained by a blue shift of the absorption band of the excess electron in the course of its solvation. [1] Initially, the electron localizes in a large cavity and absorbs in the near-IR. At later delay times, the cavity contracts and the band shifts to the visible so that the TA signal in the near-IR rapidly decays (since e_{aq}^- is a weak absorber in this region) and the TA signal in the visible increases (since e_{aq}^- absorbs strongly in the red). The ratio of the maximum TA signal to the plateau value increases with the wavelength λ because the absorptivity of e_{aq}^- rapidly decreases in the same direction. The change in the TA signal is faster where a small change in the wavelength results in the large change in the TA signal, as happens in the near-IR (section 3.3). In this general outline of the spectral evolution, our study fully concurs with the previous results. However, these features *per se* do not imply that the profile of the TA spectrum remains constant during the spectral shift.

3.3. Spectral evolution.

To characterize the spectral evolution of photoelectron during its solvation, the method outlined in [section 2](#) and [Appendix A](#) has been used. For reasons explained therein, the use of this method is justified only for relatively long delay times, $t > 0.5$ ps. The spectra $S(\lambda, t)$ obtained using eq. (1) were linearly interpolated in the time domain and then integrated between the delay times t_1 and $t_2 = t_1 + \Delta t$, to obtain the average spectrum for the corresponding (t_1, t_2) window. [Figs. 5\(a\) and 6\(a\)](#) show several such spectra for electron in light and heavy water, respectively, for delay times t_1 between 0.5 and 1.2 ps ($\Delta t = 100$ fs). [Figs. 5\(b\) and 6\(b\)](#) show the spectral evolution at later delay times, from 1.3 to 2.7 ps ($\Delta t = 200$ fs). For comparison, the spectrum of a fully thermalized, solvated electron in H_2O and D_2O is indicated by a bold line. For $t > 1$ ps, the spectral evolution of the electron in light water ([Fig. 5\(b\)](#)) is very similar to that in heavy water ([Fig. 6\(b\)](#)). By contrast, on the sub-picosecond time scale, near-IR spectra for electron in H_2O ([Fig. 5\(a\)](#)) look quite different from those in D_2O ([Fig. 6\(a\)](#)). See also [Fig. 8S](#) where the data of [Figs. 5\(a\) and 6\(a\)](#) are plotted vs. the photon energy.

On the short time scale (0.5-1.2 ps), the absorption band of the excess electron rapidly shifts to the blue. As the band shifts, the spectrum narrows on both sides of the maximum ([Fig. 8S](#)). At $t = 1$ -1.2 ps, the position E_{\max} of the absorption maximum almost reaches its equilibrium value. For $t > 1.2$ ps, the band maximum is "locked", however, the spectral evolution continues: on the red side, the absorption line becomes narrower and on the blue side, it becomes broader ([Figs. 5\(b\) and 6\(b\)](#)). Thus, there are two distinctive regimes in the spectral evolution of the electron: (i) the "fast (sub-picosecond) regime", in which the spectral features are dominated by the band shift to the blue and overall spectral narrowing and (ii) the "slow (> 1 ps) regime", in which the spectral evolution is dominated by small-scale spectral transformations occurring after E_{\max} reaches its equilibrium value.

To better characterize the latter regime, the experimental TA spectra were fit to the same Lorentzian-Gaussian curves used to simulate the spectrum of hydrated electron:

$$S(E) = \left(1 + \left[\left(E - E_{\max}\right)/W_L\right]^\nu\right)^{-1} \text{ for } E > E_{\max}, \quad (2)$$

$$S(E) = \exp\left(-\left[\left(E - E_{\max}\right)/W_G\right]^2\right) \text{ for } E < E_{\max} \quad (3)$$

where E is the photon energy (the spectrum $S(E)$ is normalized at the band maximum at $E = E_{\max}$), $\nu=2$ is the exponent, and W_L and W_G are the Lorentzian and Gaussian widths, respectively. Each spectrum $S(E,t)$ averaged over the $(t_1, t_1 + \Delta t)$ window has been fit to eqs. (2) and (3) using the least squares optimization (with a floating scaling factor), and the optimum parameters E_{\max} , W_L , and W_G were plotted vs. the delay time t_1 ($\Delta t=30$ fs slices). The resulting plots are shown in Fig. 7.

It is obvious from these plots that the increase in the band energy E_{\max} is much faster than the decrease in the Gaussian width W_G (compare Figs. 7(a) and 7(b)). For $t>0.5$ ps, both of these parameters exponentially approach their respective equilibrium values E_{\max}^∞ and W_G^∞ . For E_{\max} , the corresponding first order rate constant is ca. 3.1 ps^{-1} (which compares well with other estimates [1]). For the Gaussian width W_G , the time constants are $1.62 \pm 0.4 \text{ ps}^{-1}$ for H_2O and $1.45 \pm 0.2 \text{ ps}^{-1}$ for D_2O . It is this large difference in the corresponding time constants that accounts for the occurrence of the "slow regime" discussed above: for $t>1-1.5$ ps, E_{\max} is already very close to E_{\max}^∞ , whereas W_G still changes, being 50-100 meV greater than W_G^∞ . Based on this observation, one can globally fit the time evolution for the entire red wing of the electron spectrum $S(E,t)$ for $t>1$ ps using eq. (3) with $E_{\max}(t) = E_{\max}^\infty$ and

$$W_G(t) = W_G^\infty + (W_G^{\max} - W_G^\infty) \exp(-t/\tau_G) \quad (4)$$

where W_G^{\max} is the Gaussian width extrapolated to $t = 0$ and τ_G is the time constant of the spectral narrowing. In Figs. 8 and 9 least-squares fits to the $S(E,t)$ kinetics for electron in

light and heavy water, respectively, are shown for traces obtained between 0.85 and 1.3 μm (see also Figs. 9S and 10S). As seen from these plots, despite having only two adjustable parameters, W_G^{\max} and τ_G , eqs. (3) and (4) give surprisingly good approximation to these traces. The following estimates were obtained for these two parameters (95% confidence limits): $W_G^{\infty}=1.18\pm0.04$ eV and $\tau_G=0.56\pm0.01$ ps (for H_2O) and $W_G^{\infty}=1.2\pm0.03$ eV and $\tau_G=0.64\pm0.01$ ps (for D_2O). Thus, in agreement with the analysis given in Fig. 7(b), the spectral narrowing in D_2O is slower than in H_2O , by ca. $15\pm5\%$.

Fig. 7(c) shows the evolution of the Lorentzian width W_L of the absorption line as a function of the delay time t_1 . After the first 1 ps, this width slowly increases from 0.4 to 0.5 eV, in approximately the same fashion for light and heavy water. When the integral under the spectrum profile is plotted vs. the delay time (Fig. 7(d)), it is almost constant with time ($\pm10\%$), suggesting that in the "slow regime", the oscillator strength of the transition does not change with time: the narrowing on the red side is compensated by the broadening on the blue side. Though, it is difficult to establish this constancy accurately because the TA spectrum on the blue side is followed to $\lambda=0.4$ μm only.

We turn to the evolution of the spectra on the short time scale (0.5-1.2 ps). A curious feature of sub-picosecond TA spectra shown in Figs. 5(a) and 6(a) is an "isosbestic point" at 0.85 μm observed both in light and heavy water. [1] On closer examination, this feature does not constitute a true isosbestic point since the TA spectra obtained at different delay times do not pass through any particular point of the e_{aq}^- spectrum within the confidence limits of our measurement. Some authors [2] view this feature as evidence for the existence of two or more types of pre-solvated electron coexisting at short delay time; the observed spectral dynamics is treated in terms of

separate electron states with time-dependent spectra. [] Such elaborate schemes are impossible to falsify; little in our data suggests that these many-state models might be correct:

The largest impetus for the two-state model of the electron solvation was given by the pioneering studies of Gauduel and coworkers [] who observed a broad, short-lived component at 0.9-1.3 μm for the electron in H_2O that decayed in the first picosecond after the multi- 310 nm photon ionization. The overlap between this short-lived spectral component with the spectrum of thermalized electron was thought to account for the "isosbestic point". Since the pump pulse was quite wide (> 500 fs fwhm), [] this near-IR feature was observed well within the duration of the excitation pulse. Subsequent studies that used shorter pump pulses [] failed to reproduce this near-IR feature. For the electron in D_2O , the progression of the TA spectra in Fig. 6(a) has the same general appearance as that observed by Pépin et al. following multi- 600 nm photon ionization of heavy water []. Their spectra, in turn, are qualitatively similar to the recent data of Ulterreiner and co-workers [] and Bradforth and coworkers [] for the electron in H_2O . Either the near-IR feature observed by Gauduel and co-workers [] is very short-lived (and, therefore, requires a relatively long excitation pulse to be observed against the background from a more stable solvated-electron state) or it is caused by nonlinear absorption (section 2).

The TA spectra obtained in this study within the duration of the excitation pulse also exhibit a diffuse absorption band in the near IR. In Fig. 11S, the spectra $S(E,t)$ for the electron in D_2O shown for the 0-250 fs and 250-500 fs time windows. The vis data were excluded from the plot due to the strong contribution from nonlinear absorbance that interferes with the measurement. While using the method of eq. (1) at these short delay times is not justified, the resulting spectra closely resemble the ones reported by Migus et al. [] and Gauduel []. In Fig. 13S, a near-IR spectrum obtained in the point-to-

point fashion within the last 10% of the duration of the 200 nm photoexcitation pulse is shown for the electron in D₂O (no normalization used). Once more, this near-IR spectrum is flat across the entire band; such a spectrum would be compatible with the existence of a short-lived species that strongly absorbs at $\lambda > 0.9 \mu\text{m}$. The transformation of this TA spectrum to that shown in Fig. 6(a) is very rapid, and we conclude that the coincidence of the excitation and probe pulses in time is needed to observe this diffuse absorption band. Our data are insufficient to make the choice between the two possibilities discussed above (nonlinear absorbance vs. extremely short-lived species), and we leave the question open.

Recently, Laenen et al. [] obtained the TA spectra in near- and mid-IR after bi-266 nm photonic ionization of liquid H₂O and D₂O (see Fig. 2 and 4 therein). In H₂O, a broad absorption band from a short-lived intermediate (which the authors identify as "wet" electron) with the lifetime of 0.54 ps was observed at 1.5-1.7 μm . In D₂O, this band is red-shifted to 2 μm (still, the absorbance at 1.2 μm is ca 30% of the maximum). It is not clear from the published data how this feature evolves for $t > 0.5$ ps. Laenen et al. [] give an estimate of 3×10^4 and $5 \times 10^4 \text{ M}^{-1} \text{ cm}^{-1}$ for the molar absorptivity of the "wet" electron at 1.2 and 1.6 μm , respectively (in D₂O). Then, for these two probe wavelengths, a "wet" electron with a lifetime of 0.5-0.6 ps would yield a TA signal at $t=0.5$ ps which comprises 30-80% of the absorption signal from a fully hydrated electron (with the molar absorptivity of $2 \times 10^4 \text{ M}^{-1} \text{ cm}^{-1}$ at the band maximum). No such TA signal was observed in our study.

Instead, two features indicated by arrows in Fig. 5(a) were observed for the electron in light water: the 1.15 μm peak and the shoulder at 1.3-1.4 μm . Both of these features fully decay within the first picosecond after the photoionization, and their decay kinetics appear to be similar. Subtracting the 1.15 μm trace from the half-sum of the 1.1

and 1.2 μm traces, one obtains a kinetic profile that decays with a time constant of 0.2-0.3 ps, which is roughly the same time scale as that for the shift of the band maximum. The shoulder observed for $\lambda > 1.3 \mu\text{m}$ might be the extension the 1.4-1.8 μm feature (from the putative "wet" electron) observed by Laenen et al. [1] It also looks similar to the 1.3 μm feature observed by Miguš et al. [2] (0.24 ps life time was estimated for this feature therein).

We believe that these two features are not artifacts of the spectral reconstruction procedure described in section 2 (which is also suggested by a reasonable agreement with the previous studies); however, such a possibility cannot be excluded. Since both of these features are observed in the region where liquid H_2O has vibration overtones, the concern is that the long-lived "absorbance" signal used for normalization of the TA kinetics is from the heat induced by the absorption of UV light. The control experiments demonstrated that e_{aq}^- scavenging by 1 M acid removes > 90-95% of the 1.0-1.3 μm signal, i.e., at most 5-10% of this long-lived TA signal could be from the thermal effect. This would be insufficient to account for the 1.15 μm feature which comprises ca. 20% of the TA signal at this wavelength. For the $\lambda > 1.3 \mu\text{m}$ shoulder, such a test was difficult to conduct and we cannot discount the thermal effect entirely. It is, however, unlikely that the dynamics of such an effect would closely follow the dynamics of the 1.15 μm feature.

4. Discussion.

4.1. Long-term kinetics and the isotope effect.

Fitting the geminate recombination kinetics of e_{aq}^- generated by two 200 nm photon excitation of liquid water (section 3.1) using the IRT model [1] suggests a narrower initial electron distribution $P(r)$ in heavy water: $\sigma_G = 2.1 \text{ nm}$ for D_2O vs. $\sigma_G = 2.4 \text{ nm}$ for H_2O . While the quality of the kinetic data is (relatively) poor and it is impossible to put

confidence limits on these estimates, it is clear from Fig. 1 that only IRT curves with $\sigma_G(D_2O) < \sigma_G(H_2O)$ can account for the data.

This result is surprising since under our photoexcitation conditions (12.4 eV total excitation energy), direct ionization of the solvent (i.e., photostimulated ejection of the electron directly into the conduction band of liquid water) is thought to prevail. [1] Due to the smaller vibration energy of accepting O-D modes and, therefore, less efficient inelastic scattering of the extended-state (quasifree) electron, it has been expected that the thermalization of the conduction band electron in D₂O is less efficient and the average thermalization path is longer than in H₂O. [2]

Recently, Sander et al. [3] have analyzed the existing data on the H/D isotope effect $\alpha_{H/D} = \Omega_r(H_2O)/\Omega_r(D_2O) - 1$ for the probability Ω_r of electron recombination at $t = \infty$ as a function of the total excitation energy. They suggested that the switchover from positive to negative $\alpha_{H/D}$ with the increasing energy (which is observed between 9.5 and 10 eV) reflects a competition between the photoinduced electron transfer to a pre-existing trap (that prevails below 9.5 eV) and autoionization of water (that prevails above 9.5 eV). The latter is initiated by a *bound-to-bound* transition to a short-lived excited state; the latter promptly dissociates yielding a conduction band electron. These authors predicted the second change of the sign of $\alpha_{H/D}$, from negative to positive, when the total excitation energy exceeds ca. 11 eV and direct ionization (which involves a *bound-to-continuum* transition) prevails. Pulse radiolysis data do suggest that at some excitation energy the distribution $P(r)$ is wide ($\sigma_G \approx 2-3$ nm) and $\sigma_G(D_2O) > \sigma_G(H_2O)$. [4] However, this general result does not indicate what photon energy is required for such an electron distribution to occur: the required energy might be so high that more than one electron is generated per excitation event (the average energy needed for water ionization in radiolytic spurs is 20-25 eV [5]).

At first glance, our 12.4 eV (2 x 200 nm) data lend support to the suggestions made by Sanders et al. [3]: $\alpha_{H/D} \approx 0$ (in agreement with the predicted second switchover) and the widths σ_G compare well with those in the radiolytic spurs (suggesting the onset

of direct photoionization). On the other hand, even at this high excitation energy the distribution of electrons in D₂O is 13% narrower than in H₂O; this difference is comparable to 15% obtained by Sanders et al. for 10 eV photoexcitation [1] (at which the autoionization is supposed to prevail). It appears, therefore, that the basic premises of Sanders et al., [1] *viz.* (i) the prevalence of the direct ionization above 11 eV and (ii) a broader electron distribution in D₂O vs. H₂O attained in the course of direct ionization - are not supported by our results. Either the direct ionization does not prevail at 12.4 eV or it does not result in a longer thermalization path for D₂O. Both of these possibilities hint at a complex picture of water ionization at high excitation energy.

There have been other results suggesting such a complexity. Synchrotron radiation studies of Brocklehurst [2] reveal that the delayed luminescence from recombination of geminate ion pairs generated by vacuum UV photoexcitation of a viscous hydrocarbon squalane continuously change between 10 and 25 eV, well above the threshold energy at which the direct ionization would prevail in this liquid. The observed change in the recombination dynamics indicates continuous broadening of the electron distribution with the increasing energy. No such broadening is observed for photoionization of aromatic solutes in liquid alkanes; the width of the distribution stabilizes at 3 eV above the ionization threshold. [2] These results suggest that in squalane, the direct ionization competes with some other photoionization mechanism, even at these high photon energies. [2] The magnetic field effect data of Brocklehurst [2] and Jung and coworkers [3] provide evidence for the existence of an ionization channel through which the singlet correlation between the radical ions in the geminate pair is rapidly lost; spin-orbit interaction in the excited bound state of the solvent (which mediates the autoionization) has been suggested as such a channel. [2] This loss of spin correlation is quite notable between 11 and 16 eV, at the very onset of the direct ionization. [2] Perhaps, the distinction between the direct ionization and autoionization is not as clear-cut as suggested by Sanders et al.: [1] both photoprocess compete well above the postulated 11 eV threshold.

4.2. Spectral evolution in the "slow regime": phenomenology.

Why did the "slow regime" of the spectral evolution observed in section 3.3 escape the attention of other workers? As explained in the Introduction, in most of the previous pump-probe studies, the spectral sampling was too sparse and the S/N ratio was inadequate to observe the subtle changes in the spectral shape. Furthermore, the best-quality spectral data were fit using the "continuous shift" model; for obvious reasons, such an analysis fails to identify the occurrence of the small-scale change in the spectral profile. Lastly, the "slow regime" has actually been observed previously, by Pépin et al. [1]. These workers carried out a Gaussian-Lorentzian analysis similar to that outlined in section 3.3 for the electron generated by multiphoton ionization of liquid D₂O ($\lambda=0.5$ to 1.4 μm). As seen from Figs. 3 and 4 in ref. [1], the Gaussian width systematically decreased with delay time, much like the same quantity in Fig. 7(b). To account for this apparent contradiction with the "continuous shift" model, Pépin et al. [1] postulated that the electron spectrum slides over a "supplementary component" from an unknown species with the life time of 2 ps that absorbs at 0.8-1.2 μm (see Fig. 6 therein). No other group was able to identify this species.

Subsequently, Jay-Gerin and co-workers [1] reinterpreted these observations in terms of a more fanciful two-state model of electron solvation (the "hybrid model" [1]). In the latter model, there are two electron species, the "wet" electron and the "solvated" electron. Both of the corresponding spectra undergo the "continuous shift" to the blue on the subpicosecond time scale. The more energetic of these species ("wet" electron) also rapidly converts to a more stable one ("solvated" electron). Analogies to the electron solvation in aliphatic alcohols were drawn to substantiate the use of this model for electron solvation in water. [1] The "hybrid" model assumes that the profile of the electron spectrum does not change during the solvent relaxation (when the "continuous shift" occurs) or, at the very least, it is a Gaussian-Lorentzian function. No justification has

been given for either one of these basic assumptions, and the "hybrid model" has as much fidelity as the "supplementary component" model. Naturally, such models are impossible to falsify because arbitrary properties can be assigned to the progenitors of various components.

We believe that it would be more appropriate to interpret these observations at their face value, i.e., as evidence that the spectrum profile of the electron does evolve with time and, at short delay times, strongly deviates from the Gaussian-Lorentzian form. As shown in section 3.3, the entire set of TA kinetics for the electron in H₂O and D₂O in the red and near IR can be fit using a simple spectrum-narrowing model with only two adjustable parameters.

Another concern is whether our observations can be explained using the "thermal jump" model of Keiding et al. [1] or the "cavity contraction" model of Unterreiner et al. [2]. The answer is negative, because in their predictions, these two (seemingly different) models are almost indistinguishable from the "continuous shift" model. Within the framework of these models, the change in E_{\max} is interpreted either in terms of the decrease in the local temperature around the electron [1] or the mean square dispersion of its position with respect to the cavity center [2]. As for the latter model, the shape stability is the implicit assumption, i.e., the "cavity contraction" model is a reformulation of the "continuous shift" model. The temperature jump model of Keiding et al. [1], despite its different physical context, is also a variant of the "continuous shift" model: Since the width of the e_{aq}^- spectrum change with the increasing temperature much slower than E_{\max} (see Appendix A), simulations using this model yield spectral evolution which is very similar to that given by the "continuous shift" model. Furthermore, cursory analysis of the data in Figs. 7(a) and 7(b) immediately points out to a major inconsistency: while a temperature shift of 30 K would suffice to account for the position of the band maximum

at $t=0.5$ ps, a temperature shift of 200 K would be needed to account for the width of the electron spectrum (see Fig. 3S(b)). The stated, however, refers to the parameterization of the e_{aq}^- spectra vs. temperature used by Keiding et al., [1] and this parameterization is not supported by more recent studies. [2] In particular, Bartels et al. [2] observed substantial deviations of the spectral profile of hydrated electron in hot water from the Gaussian-Lorentzian curve given by eqs. (3) and (4) with the temperature-independent parameter $\nu = 2$. They demonstrated that in hot water, the spectral profile is given by a modified eq. (3) with ν that increases with the temperature and a temperature-independent width W_L . The resulting "hot-water" spectra are increasingly flatter at the top at higher temperature. [3] (see Fig. 4S).

Given these recent developments, we re-analyzed the $S(\lambda, t)$ set in the spirit of the "temperature jump" model, using modified eq. (3) for constant W_L and time-dependent parameters E_{\max} , W_G , and ν (Appendix A). Figs. 11S and 12S(a,b,c) show the least-squares fits to the spectra and the time dependencies of the optimum parameters for electron solvation in D₂O. The remarkable feature of Fig. 12S(b) is that the Gaussian width W_G is constant for $t > 1$ ps: the entire spectral evolution can be explained in terms of a relatively slow increase in E_{\max} with a time constant of 1 ps (Fig. 12S(a)) and a concomitant decrease in ν (from 2.5 at 1 ps to the equilibrium value of 1.95, with a time constant of 0.6 ps (Fig. 12S(c)). In this model, the spectral evolution during the electron solvation is regarded as the slow spectral shift accompanied by an increase in the curvature of the spectrum at the top. Although the use of eq. (3) with constant W_L and variable ν yields as good quality fits as the previously considered model with variable W_L and constant ν (and finds equal support in the data on the temperature evolution of e_{aq}^- spectra), entirely different dynamics for E_{\max} were obtained from the least-squares fits to the same data set (compare Figs. 7 and 12S). This example illustrates the general

point made in the Introduction: the extraction of E_{\max} strongly depends on the template used to fit the data. However, even with this different functional form, the optimum parameters shown in Fig. 12S are inconsistent with the "temperature jump" model of Keiding et al.: [1] to obtain $\nu \approx 2.3$ at $t=1$ ps, a temperature jump of 250 K would be needed (Figs. 3S(a) and 3S(b)), whereas the position of E_{\max} at this delay time corresponds to a modest temperature jump of 40 K. We conclude that the "temperature jump" model is not supported by our results.

The spectral narrowing described by eq. (3) complemented by eq. (4) (Figs. 8 and 9) naturally accounts for the major trend shown in Figs. 2, 3, and 4: the greater is the difference $E_{\max}^{\infty} - E$ (> 0) for a given photon energy E , the faster is the decay of the electron absorbance at the corresponding wavelength. By increasing the bulk temperature [1] or by addition of salt, [1] it is possible to, respectively, red- or blue- shift the spectrum of hydrated electron (i.e., to decrease or increase E_{\max}^{∞}). Since the initial spectrum of pre-solvated electron does not change significantly as a function of temperature or salinity, the basic prediction of the spectrum-narrowing model is that for a fixed probe wavelength (on the red side of the e_{aq}^- spectrum), the decay of the absorption is progressively slower with the increasing temperature and progressively faster with the increasing salinity. Both of these trends are consistent with the experimental observations of Ulterreiner et al. [1] and Crowell et al. [1] (for the temperature effect) and Lian et al. [1] (for the salinity effect).

4.3. Spectral evolution: possible mechanisms.

From the theoretical prospective, the chief appeal of the "continuous shift" model is a possibility to reduce the complex spectral evolution of the electron to a single time-dependent parameter $E_{\max}(t)$ related to the average electron energy; the latter quantity may be obtained directly from molecular dynamics (MD) simulations. [1] If the

"continuous shift" model were incorrect, such an approach would be insufficient: time-resolved spectra should be simulated instead. The latter is a more complicated problem [1] which requires the detailed knowledge of the ground and excited state, transition probabilities, etc. Even for hydrated (thermally relaxed) electron, the origin of the absorption spectra is the subject of ongoing controversy and continuing research. [2] E.g., some basic features of this spectrum (e.g., homogeneous vs. inhomogeneous broadening) are still debated in the literature. [3]

The emerging consensus is that the vis and near-IR spectrum of cavity electron in liquid water is from the three partially merged $s \rightarrow p$ subbands; these subbands correspond to the three orientations of the p orbital of the final state with respect to the principal axes of the ellipsoidal solvation cavity. [4] While this simple picture is supported by numerous MD calculations, [5] hole burning absorption anisotropy experiments by Assel et al. [6] did not yield the expected polarization-depended TA dynamics. Some anisotropy was observed by Barbara and co-workers, [7] however, the depolarization dynamics were different from the theoretical predictions of Schwartz and Rossky. [8] A possible rationale for these discrepancies was proposed by Bratos and Leicknam [9] who postulated rapid (~ 10 fs) internal relaxation in the p -state manifold. Another possibility is that the experimental manifestation of the anisotropy following the $s \rightarrow p$ photoexcitation depends on the photon energy of this excitation. In particular, a single p subband was excited in the experiments of Barabra and coworkers [10] whereas in the experiments of Assel et al. [6] two overlapping subbands (with the orthogonal orientation of the p orbitals) were photoexcited simultaneously. In the latter case, the anisotropy would be more difficult to observe. Importantly, rapid decay of photon echo following the $s \rightarrow p$ photoexcitation observed by Wiersma and coworkers [11] cannot be considered

as unequivocal evidence for fast dephasing in the *p* manifold since rapid Stokes shift can also explain these data. [1]

While a clear-cut demonstration of the substructure in the electron spectrum by means of ultrafast spectroscopy is still lacking, indirect support for the *p* state nondegeneracy and slow dephasing is given by resonance Raman spectra for hydrated electron: Tauber and Mathies [2] determined the depolarization ratio across the entire Raman spectrum of e_{aq}^- in liquid H₂O and concluded that this ratio (ca. 0.3-0.5) is incompatible with a resonant transition to a *single* nondegenerate state. Their analyses [3] suggest that homogeneous broadening for e_{aq}^- is at least 100 times greater than inhomogeneous broadening [4] and the half width of the $s \rightarrow p$ band on the red side is largely determined by vibrational progressions from the five strongest modes with vibrational energies between 470 and 3100 cm⁻¹ (for H₂O).

It is apparent from these results that the overall shape of the electron spectrum is controlled by many parameters, and only advanced theory can consistently account for the spectral evolution in the course of electron solvation. As stated in the Introduction, given the previous record of kinetic modeling, we do not feel compelled to provide yet another *ad hoc* scheme "explaining" the results. Only a comprehensive, rigorous theory would be up to this task. Still, it is appropriate to speculate on the origin of the two novel features reported in this paper, namely, (i) the spectral narrowing/broadening that occurs in the "slow regime" ($t > 1$ ps) and (ii) apparent differences between the subpicosecond TA spectra for the excess electron in H₂O and D₂O.

The characteristic spectral transformations observed in the "slow regime", *viz.* narrowing of the band on the red side and broadening on the blue side, bear some resemblance to the evolution of absorption bands for electronically-excited molecules

undergoing vibrational relaxation. Such a relaxation involves nonequilibrium populations of vibrational states which according to Tauber and Mathies [1] determine the shape and the width of the e_{aq}^- spectrum. This vibrational relaxation readily explains the isotope dependence for the time constant of spectral narrowing. The time scale for the vibration relaxation in liquid water (ca. 0.75-1 ps for the O-H stretch in the room-temperature dilute HOD:D₂O) [2] compares well with the observed time scale of spectrum narrowing in our experiment.

Another possible rationale is a time-dependent change in the relative positions and weights of different p subbands, although the origin of the isotope effect is less clear in such a case. As follows from the analysis of Bartels et al., [3] the spectrum of e_{aq}^- becomes flatter at the top with the increasing water temperature. Similar changes were observed by Brodsky et al. [4] and Herrmann and Krebs [5] for methanol. The likely cause for this change is the increasing asymmetry of the solvation cavity as it grows in size in hot water. Consequently, the splitting between the three p subbands increases and the electron spectrum becomes more flat at the top. If the p subbands do define the shape of the electron spectrum in the visible and near-IR, as suggested by MD calculations, [6] the "slow regime" may be interpreted as gradual decrease in the anisotropy of the solvation cavity during its relaxation. That, in turn, suggests that the initial localization of the electron involves a highly anisotropic trap. Such an assertion is in agreement with the theoretical models of electron trapping in liquid water. [7] Indirect experimental support for this assertion is provided by the data on electron trapping in crystalline ice: quasifree electrons were shown to localize on (highly anisotropic) Bjerrum defects; [8] after this initial localization, the water structure around such a defect relaxes and the a solvation cavity gradually emerges on picosecond time scale (the resulting spectrum bears strong

resemblance to the spectrum of hydrated electron and changes little between 4 and 270 K). [1]

It seems likely that the changing anisotropy of the solvation cavity is the ultimate cause for the failure of the "continuous shift" and "temperature jump" models to capture the essentials of the spectral evolution. In these models, the environment of the electron during its solvation is assumed to have the same degree of anisotropy as fully relaxed, hydrated electron, either at the final or elevated temperature. Perhaps, the increase in the sphericity of the solvation cavity (both on sub-picosecond time scale and at later delay times) occurs in concert with the vibrational relaxation of solvent molecules forming the solvation cavity (see above); such a concerted mechanism would account for the isotope effect on the spectral narrowing.

On the subpicosecond time scale, the vibrations in water appear to have strong effect on the spectral evolution. Indeed, for light water, new spectral features were observed in the near-IR, where the water molecule has O-H stretch overtones. No such features were observed in D₂O for which these overtones are red-shifted to > 1.7 μ m. As explained in section 3.3, the thermal effect (a photoinduced change in the refraction index of water) does not appear to cause these features. Still, the vibrations of water molecules are implicated. Due to the extreme isotope selectivity, many potential candidates for the progenitors of these features, for instance, IR-absorbing *p* state electron examined theoretically by Schwartz and Rossky [2] and experimentally by Barbara and coworkers [3], can be excluded since the generation of such a species in the course of photoionization, while plausible, does not account for these specific features. We stress that our data (as well as the previous studies [4]) do not provide clear-cut evidence either against or for such an involvement. [5] The same refers to the involvement of the tentative "wet"

electron [1] and liquid-water analog of the IR-absorbing electron in low-temperature ice [2] postulated by others.

We believe that the 1.15 and 1.3-1.4 μm features for the excess electron in H_2O emerge due to collective excitation of the electronic and vibrational modes of pre-solvated electron by the IR light, when the corresponding energies are close. It is possible that the same features are present in the TA spectra of $s \rightarrow p$ excited hydrated electrons; unfortunately, no spectra in the near- and mid-IR are currently available (only 0.55-1.05 μm spectra have been reported). [3] In the photon echo and transient grating experiments of Wiersma and coworkers, a librational motion of water molecules (ca. 850 cm^{-1}) in the relaxation dynamics of electron following $s \rightarrow p$ photoexcitation was observed. Resonance Raman spectra of hydrated electron indicate strong coupling of the $s \rightarrow p$ electronic transition to the O-H stretch and bend modes. [4] Such a coupling would be expected on the theoretical grounds since the O-H groups with protons pointing out towards the cavity center comprise the core of the solvated electron. [5] Vibronic transitions in the near-IR would be another manifestation of this coupling. Specifically, we suggest that O-H vibrations can be excited when the energy of the electronic transition is close to that of the O-H stretch overtone. To our knowledge, such a possibility has not been addressed theoretically, while it is suggested by the results of the present work. In the current MD models, water is treated classically and such phenomena as vibronic coupling and vibrational relaxation for hydrated electron cannot be studied. The results discussed above suggest that these phenomena might play a prominent role in the electron solvation dynamics; hence, more advanced models might be needed.

5. Conclusion.

The evolution of vis and near-IR TA spectra for pre-solvated electron following biphotonic excitation of the room-temperature light and heavy water has been studied.

For two 200 nm photon excitation process, the geminate recombination within the first 5-10 ps is negligible. A method based on the normalization of kinetic traces by the spectrum of hydrated electron was implemented to reliably reconstruct the TA spectra for delay times $t > 0.5$ ps (for a 300 fs fwhm photoexcitation pulse).

Two regimes of the spectral evolution were observed. In both of these regimes, the spectral profile changes with delay time; the "continuous blue shift" [1] and "temperature jump" models [2] that assume the constancy of this spectral profile (as the electron spectrum shifts to the blue) are not supported by our data. On the sub-picosecond time scale, the band maximum systematically shifts to the higher photon energy and the spectrum narrows (Figs. 5(a), 6(a), and 8S). At later delay times ($t > 1$ ps), the position of the band maximum is "locked", but the spectral profile continues to change, by narrowing on the red side and broadening on the blue side (Figs. 5(b) and 6(b)). The oscillator strength of the transition is constant within 10% during this relatively slow, small-scale spectral transformation. The spectral narrowing can be accounted for by a two-parameter model in which the width of the Gaussian half-line exponentially decreases with the delay time. The time constant of this narrowing is ca. 0.56 ps for H₂O and 0.64 ps for D₂O, respectively.

In the first picosecond after photoionization, two new features (the 1.15 μ m band and 1.4 μ m shoulder) were observed in the near-IR spectra for the electron in H₂O; these two features were not observed for the electron in D₂O. These two features are observed in the same region where O-H overtones appear in the spectra of liquid water. While it cannot be entirely excluded that these two features are artifacts of the data analysis (despite good agreement with some reported spectra [3]), it seems more likely that these bands are genuine and originate through the vibronic transitions of pre-solvated electron. The isotope-dependent narrowing/broadening of the absorption band of the electron for $t > 1$ ps can be interpreted as evidence for the occurrence of vibrational relaxation in the water molecules lining the solvation cavity. In both of these regimes, continuous decrease in the size and anisotropy of the solvation cavity causes a time-dependent blue shift and decrease in the splitting between the three *p* subbands of the electron. These two trends would qualitatively account for the observed spectral evolution.

Since the current theories of hydrated electron in liquid water do not involve the quantum degrees of freedom for vibrations in water molecules, the vibrational relaxation and the vibronic coupling hinted at by our results cannot be presently modelled. Further development of the theory might be necessary for a self-consistent explanation of the spectral evolution during the thermalization/localization/solvation process.

The geminate recombination kinetics for hydrated electrons generated by absorption of two 200 nm quanta (12.4 eV total energy) by light and heavy water are very similar. Kinetic analyses within the framework of the IRT model suggest that the initial distribution of distances between the electron and its geminate partners in D₂O is narrower than in H₂O. Since the opposite trend is expected in the regime where direct ionization prevails, we speculate that autoionization of water still competes with the direct ionization at this high excitation energy. The latter ionization mechanism has been thought to prevail when the total excitation energy is greater than 11 eV [1] (the conduction band in water is typically placed between 9 and 10 eV [2]). While this result is unexpected, it is consistent with the previous observations of competing ionization channels in the vacuum UV photoexcitation of molecular liquids. [3]

6. Acknowledgement.

We thank Prof. B. J. Schwartz of UCLA and Drs. C. D. Jonah and D. M. Bartels of ANL for useful discussions. The research at the ANL was supported by the Office of Science, Division of Chemical Sciences, US-DOE under contract number W-31-109-ENG-38.

Supporting Information Available: (1.) A PDF file containing (a) Appendix A. The absorption spectrum of hydrated electron, (b) Appendix B. Instruction for the retrieval of kinetic data from the supplied ascii file, (c) captions to Figs. 1S to 13S, and (d) Figs. 1S to 13S; (2.) A 288 Kb ascii file named "[H2O_D2O_traces.txt](#)" containing digitized kinetic traces $S(\lambda,t)$ for the electron in H₂O and D₂O. This material is available free of charge via the Internet at <http://pubs.acs.org>.

References

*) Such an interpretation, however, is not the only possible. In the theory of Brodsky and Tsarevski, [1] the flattop profiles are explained quite differently. Furthermore, the recent MD calculations of Borgis and coworkers [2] using floating Gaussian orbitals did not reproduce this feature though the p subbands were implicit in these calculations.

Figure captions.

Fig. 1.

Geminate recombination dynamics of hydrated electrons generated by 2×200 nm photoexcitation of neat liquid H_2O and D_2O at 25°C . The photoinduced optical density ΔOD_{800} (observed at $\lambda = 800$ nm and normalized at $t=5-10$ ps) is plotted vs. the delay time t on the logarithmic time scale. Note that the origin of the vertical axis is at 80% recombination efficiency. The data for heavy water are indicated using open circles and diamonds, for light water - open squares and triangles. The vertical bars indicate 95% confidence limits. Two series of data obtained at $2 \mu\text{J}$ and $5 \mu\text{J}$ excitation power (*circles and squares and diamonds and triangles*, respectively) are shown to illustrate the constancy of the time profile with the 200 nm light radiance in the explored excitation regime (compare with Fig. 2S(b)). All four normalized kinetics are identical within the confidence limits. Solid lines are IRT model simulations. The simulation parameters are given in Table 1S in the supplement. The black solid line is the simulation for light water with $\sigma_G = 2.4$ nm (average separation of 3.83 nm); traces (i), (ii), and (iii) are simulations for heavy water for $\sigma_G = 2.1, 2.4$, and 2.7 nm, respectively.

Fig. 2

A family of kinetic traces $S(\lambda, t)$ (section 2 and eq. (1)) for electron generated by bi- 200 nm photonic ionization of the room-temperature light water. The magnitude of the hydrated electron spectrum at the maximum is taken as unity. The probe wavelength λ (500 to 1350 nm) is given in the color scales to the right of the plots. The vertical bars are 95% confidence limits. The "spike" near the kinetic origin in (a) is from nonlinear absorbance due to simultaneous absorption of 200 nm and probe photons. The sigmoid curve in (b) is the integral of the response function of the system (which is shown by a shaded curve in (c)).

Fig. 3

Same as Fig. 2, for heavy water. Only 500 to 1050 nm data are shown.

Fig. 4

Same as Fig. 2, for heavy water. Only 1100 to 1700 nm data are shown. In (b), the vertical scale is expanded to illustrate nonzero plateau attained by the kinetics at $t > 3$ ps.

Fig. 5

TA spectra $S(\lambda, t)$ for electron in light water at different delay time intervals $t = (t_1, t_1 + \Delta t)$. The delay times t_1 are given in the plots. For (a) $\Delta t = 100$ fs, for (b) - 200 fs. The maximum TA signal from the hydrated electron $S(\lambda) = S(\lambda, t = \infty)$ is taken for unity. The solid lines in (b) are Gaussian-Lorentzian functions obtained by least-squares fits, as explained in the text (note the logarithmic vertical scale). The vertical bars are 95% confidence limits. The bold solid line is the normalized spectrum ($S(\lambda)$) of fully thermalized hydrated electron. The vertical arrows indicate previously unobserved features in the near-IR.

Fig. 6

Same as Fig. 5, for the electron in heavy water.

Fig. 7

Gaussian-Lorentzian analysis of linearly interpolated $S(\lambda, t)$ data for the electron in light (*open squares*) and heavy (*open circles*) water. Vertical bars are 95% confidence limits determined by least-squares optimization. The solid lines in (a) and (b) are exponential fits. (a) The position of the spectrum maximum, (b) Gaussian width, (c) Lorentzian width, and (d) the integral under the spectrum plotted as a function of the delay time t_1 for $\Delta t = 30$ fs.

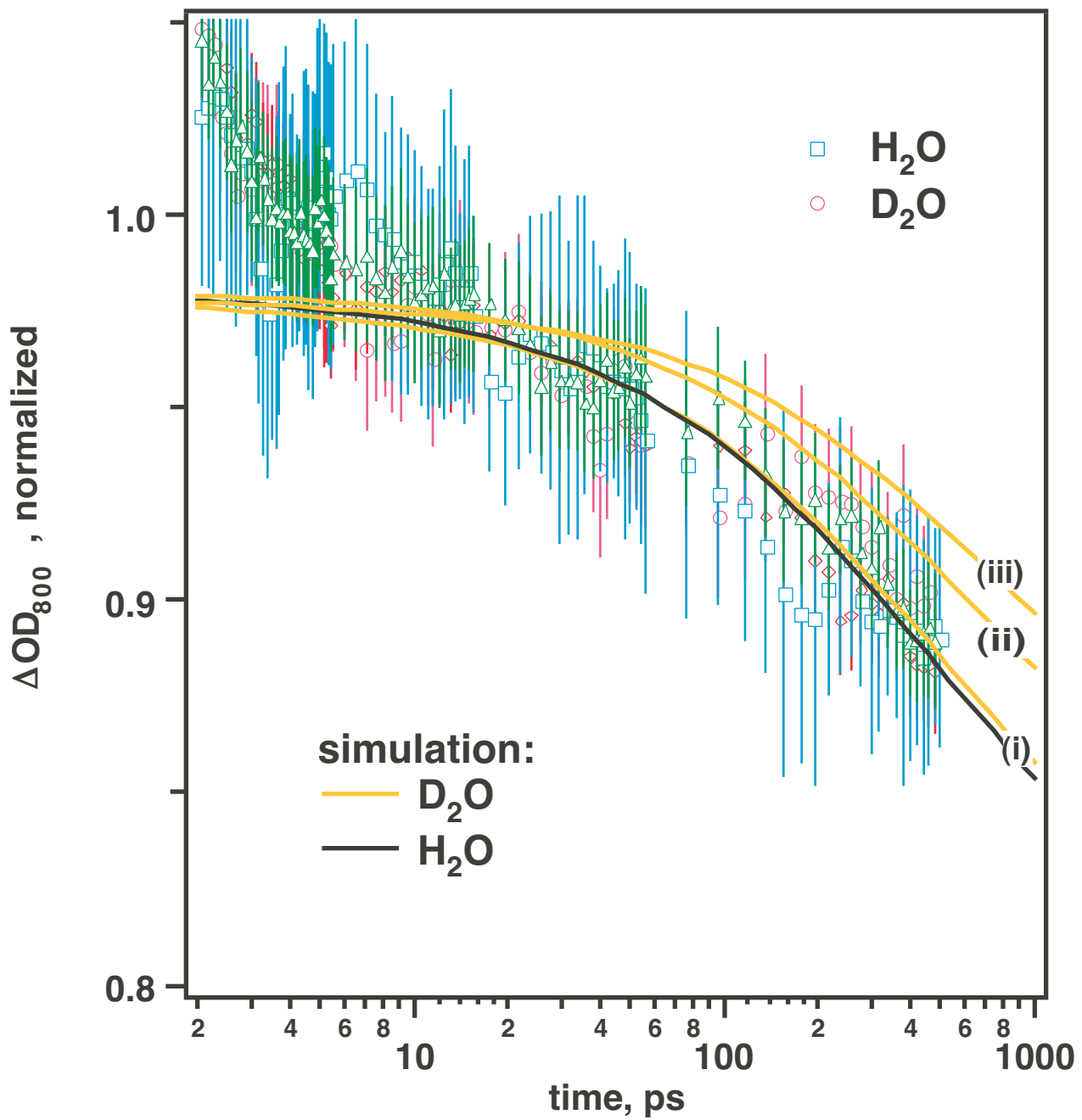
Fig. 8

"Global" least squares analysis of $S(\lambda, t)$ kinetics using the spectrum-narrowing model (eqs. (3) and (4)) for the electron in light water. The solid lines are simulated kinetics for,

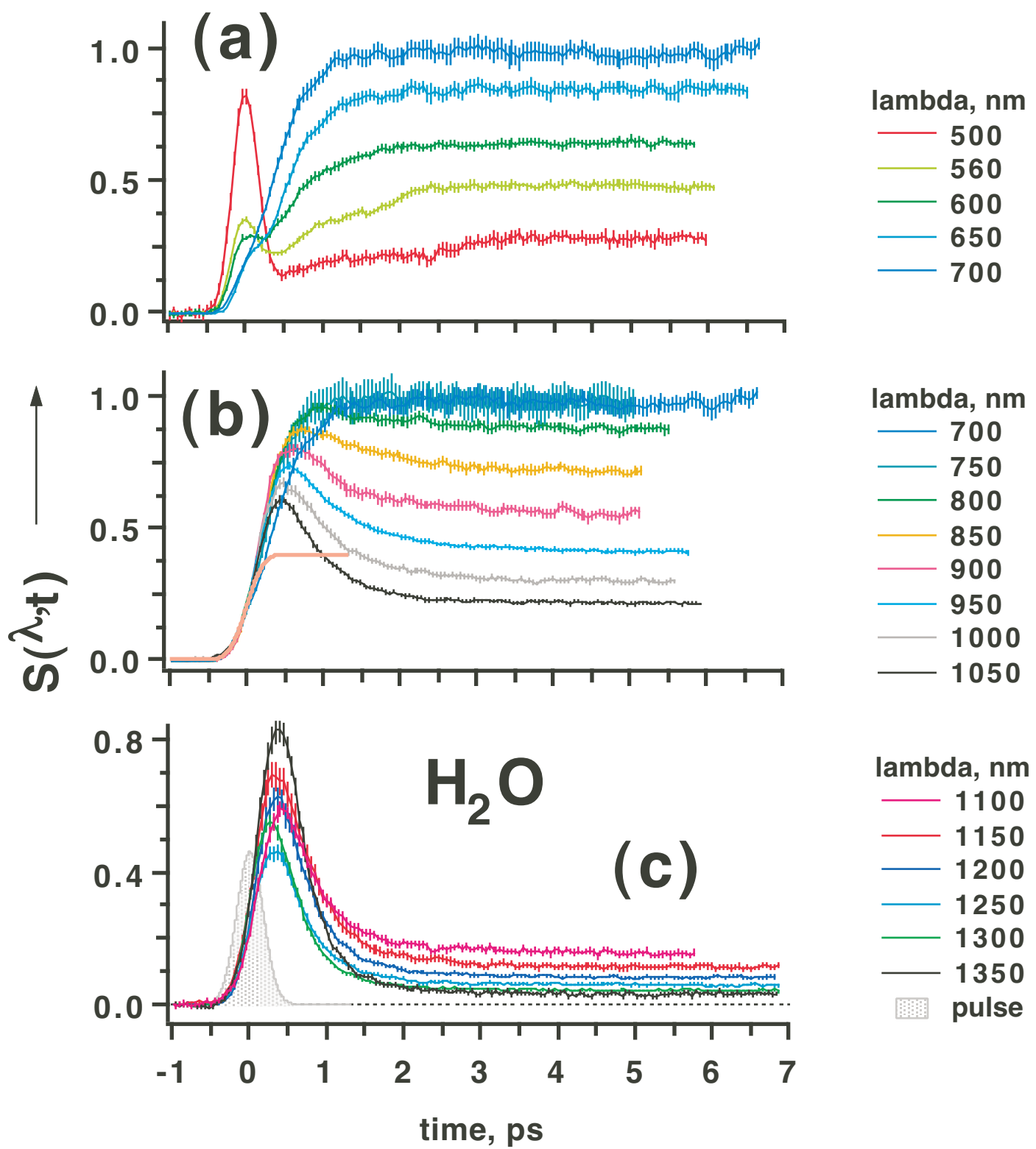
from top to bottom: $\lambda = 800, 850, 900, 950, 1000, 1050, 1100, 1200, 1250$, and 1300 nm. The vertical bars are 95% confidence limits. Fig. 9S gives the expanded version of this plot for traces with $\lambda \geq 1$ μm .

Fig. 9

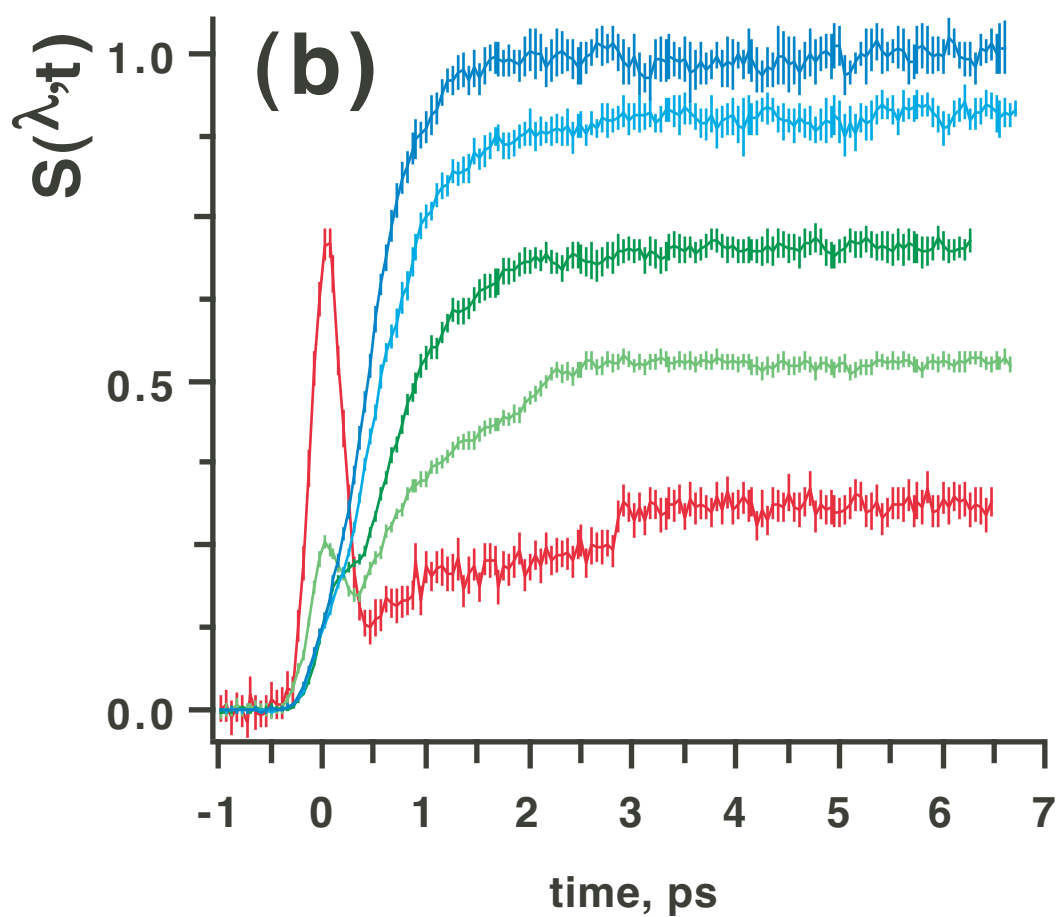
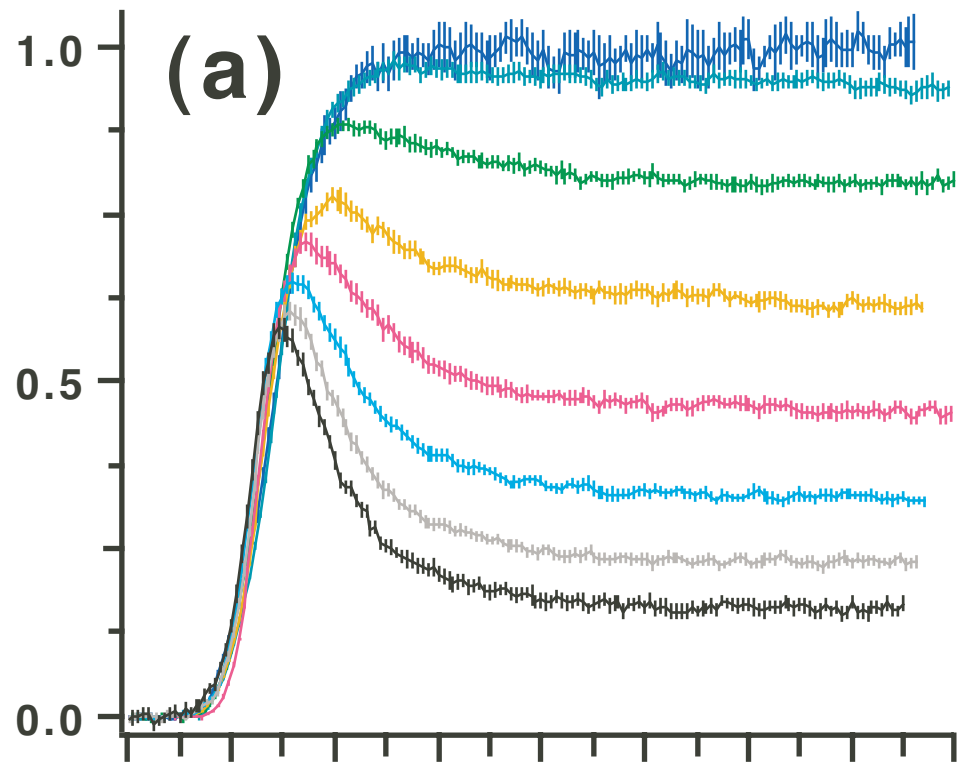
Same as Fig. 8, for the electron in heavy water. The probe wavelengths are 850, 900, 950, 1000, 1050, 1100, 1200, 1250, and 1300 nm. Fig. 10S gives the expanded version of this plot for traces with $\lambda \geq 1$ μm .



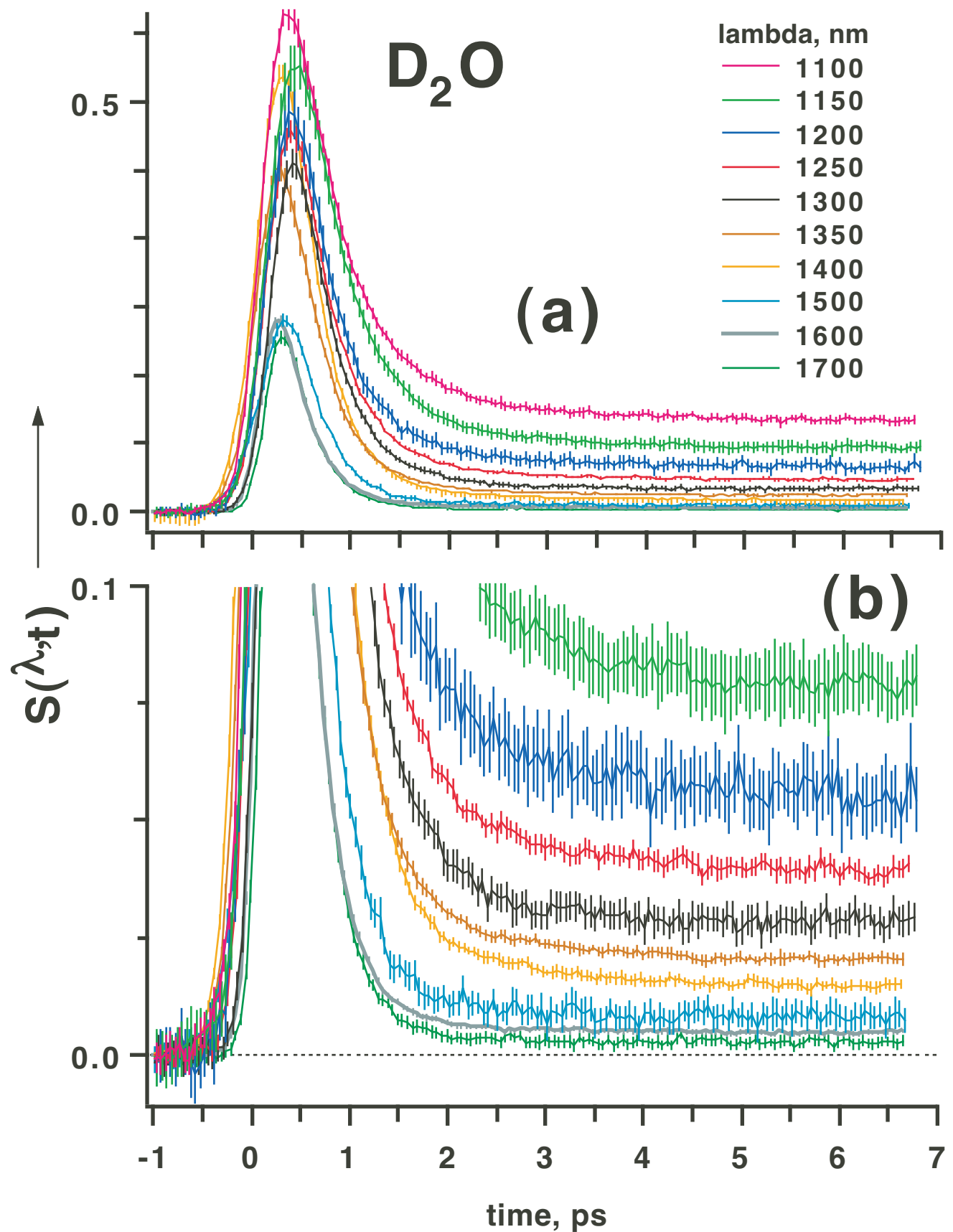
Lian et al., Figure 1



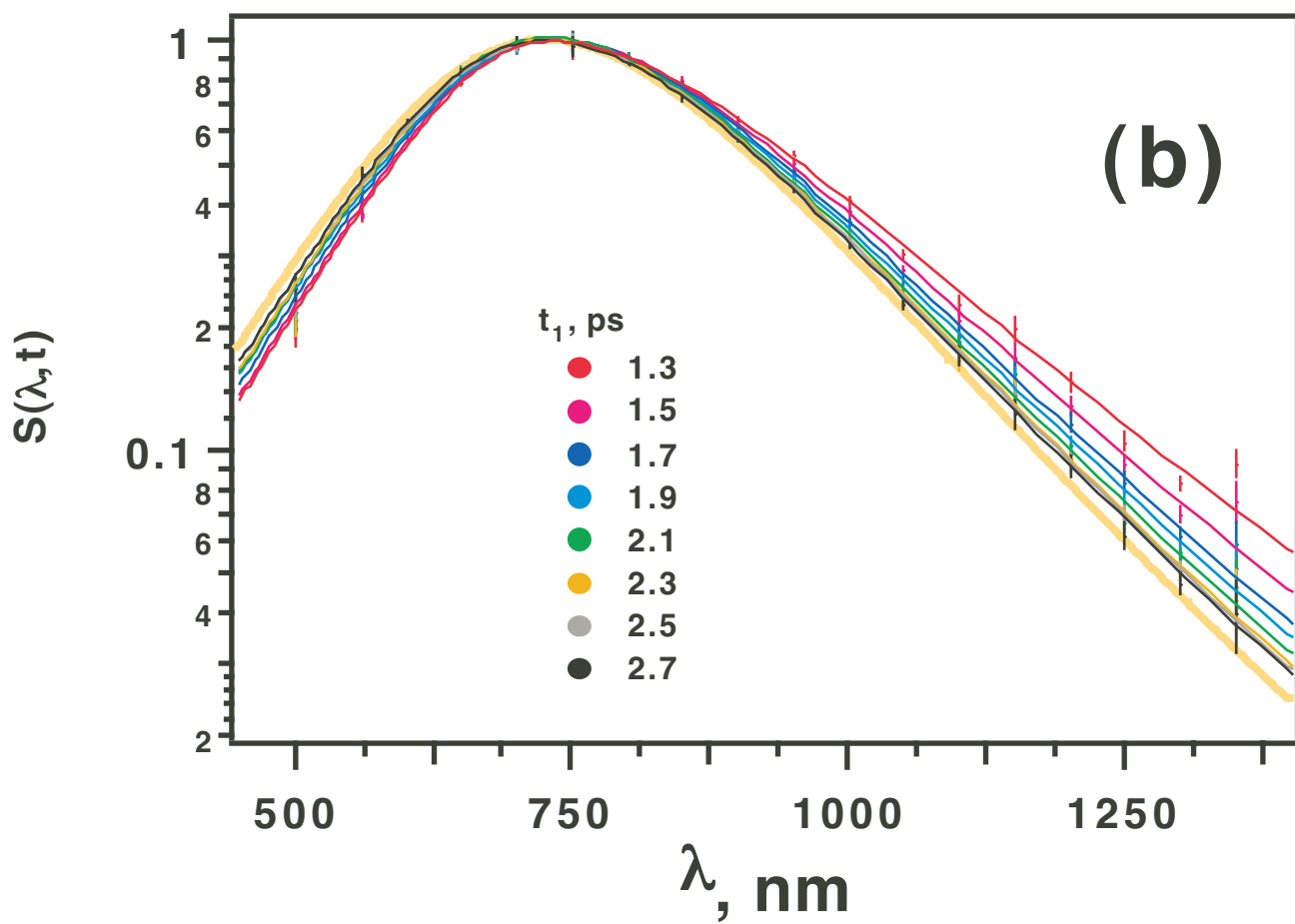
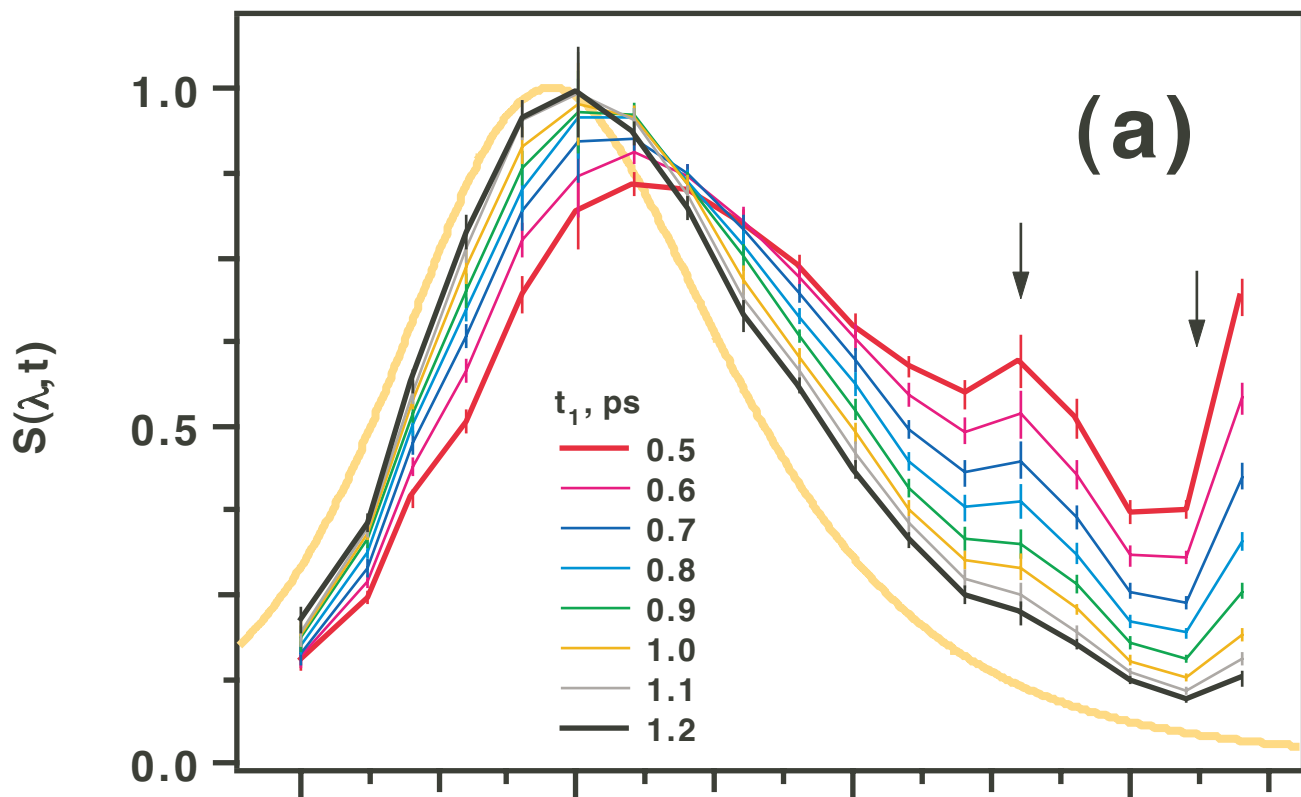
Lian et al., Figure 2



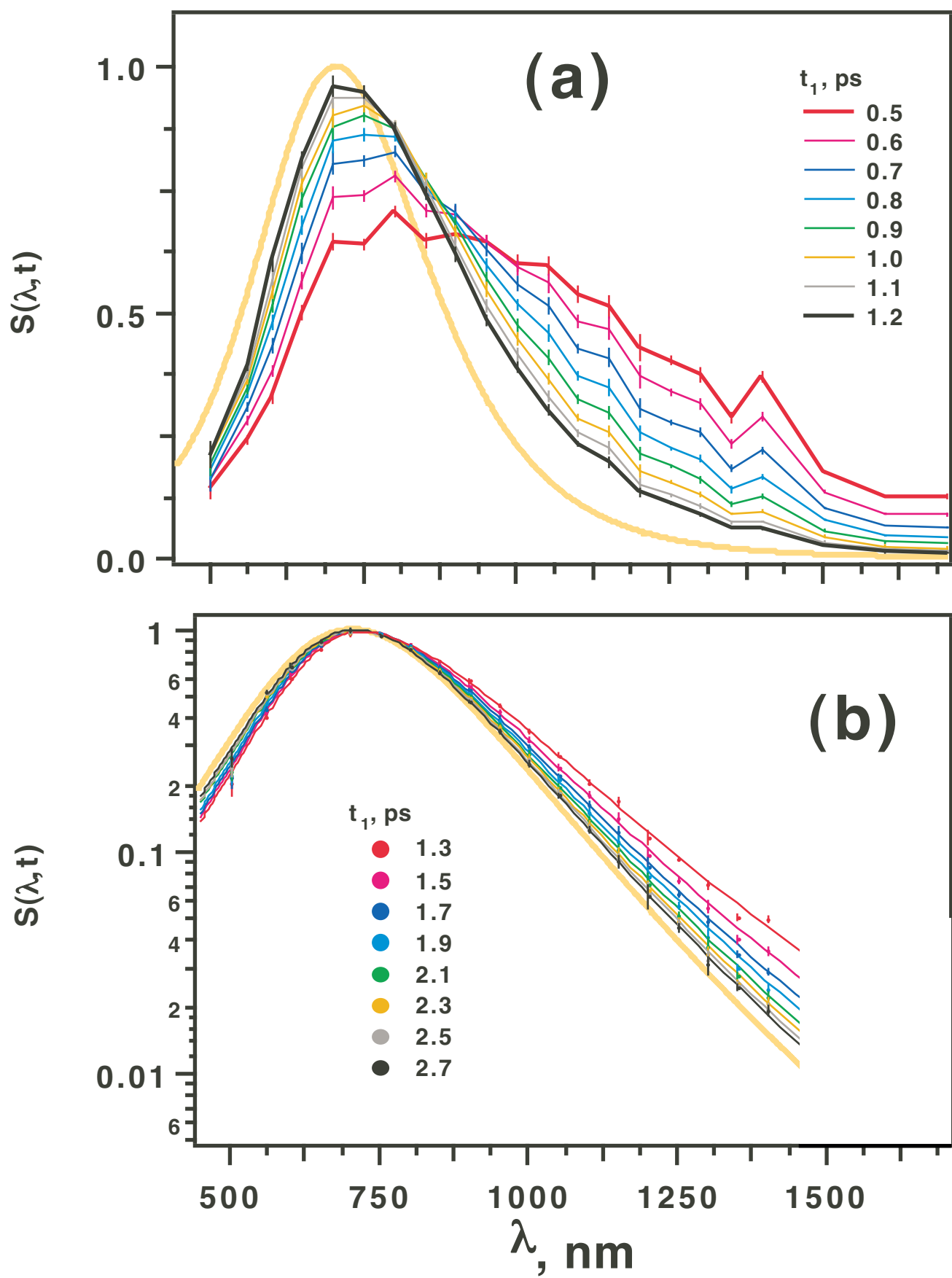
Lian et al., Figure 3



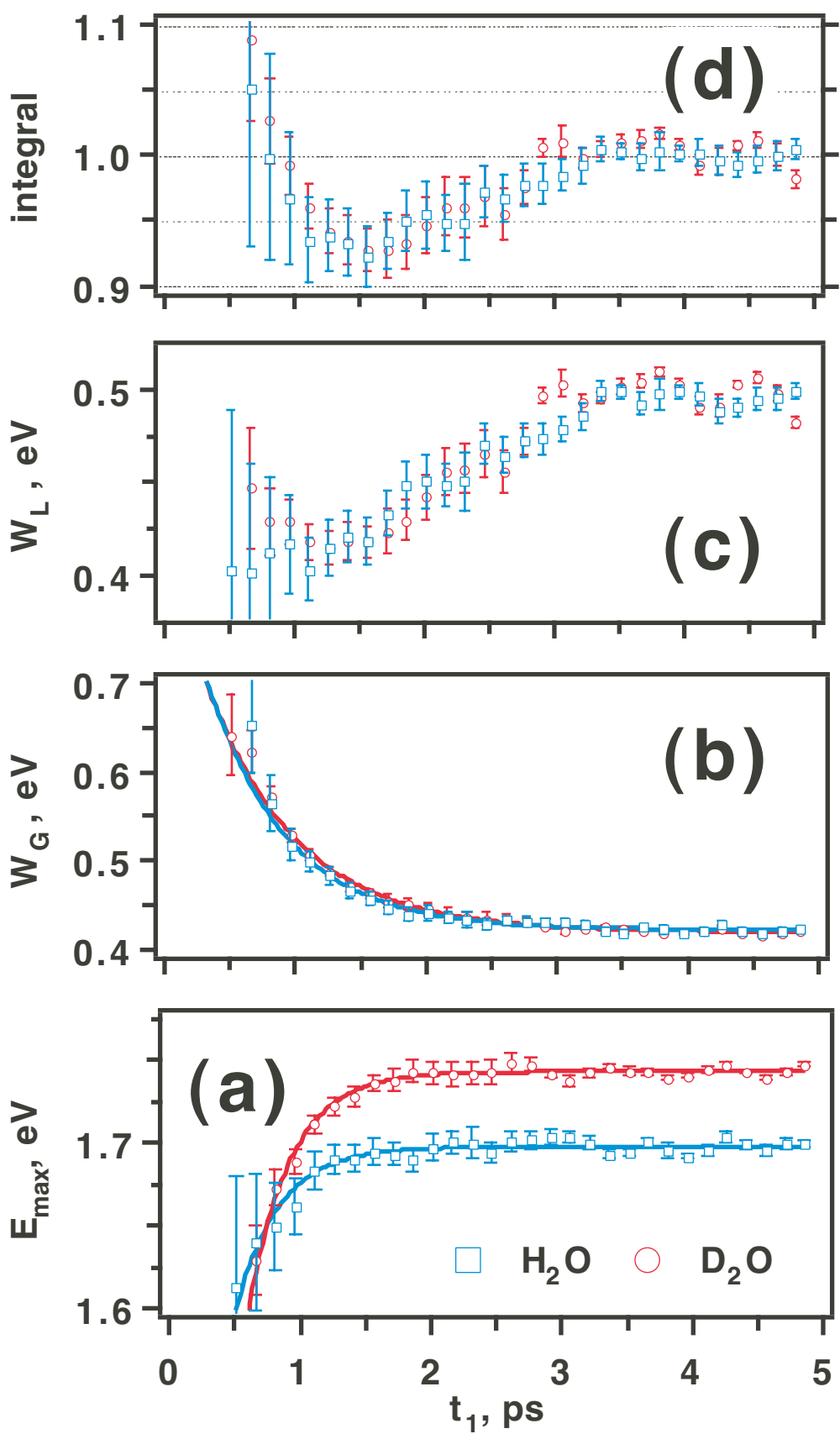
Lian et al., Figure 4



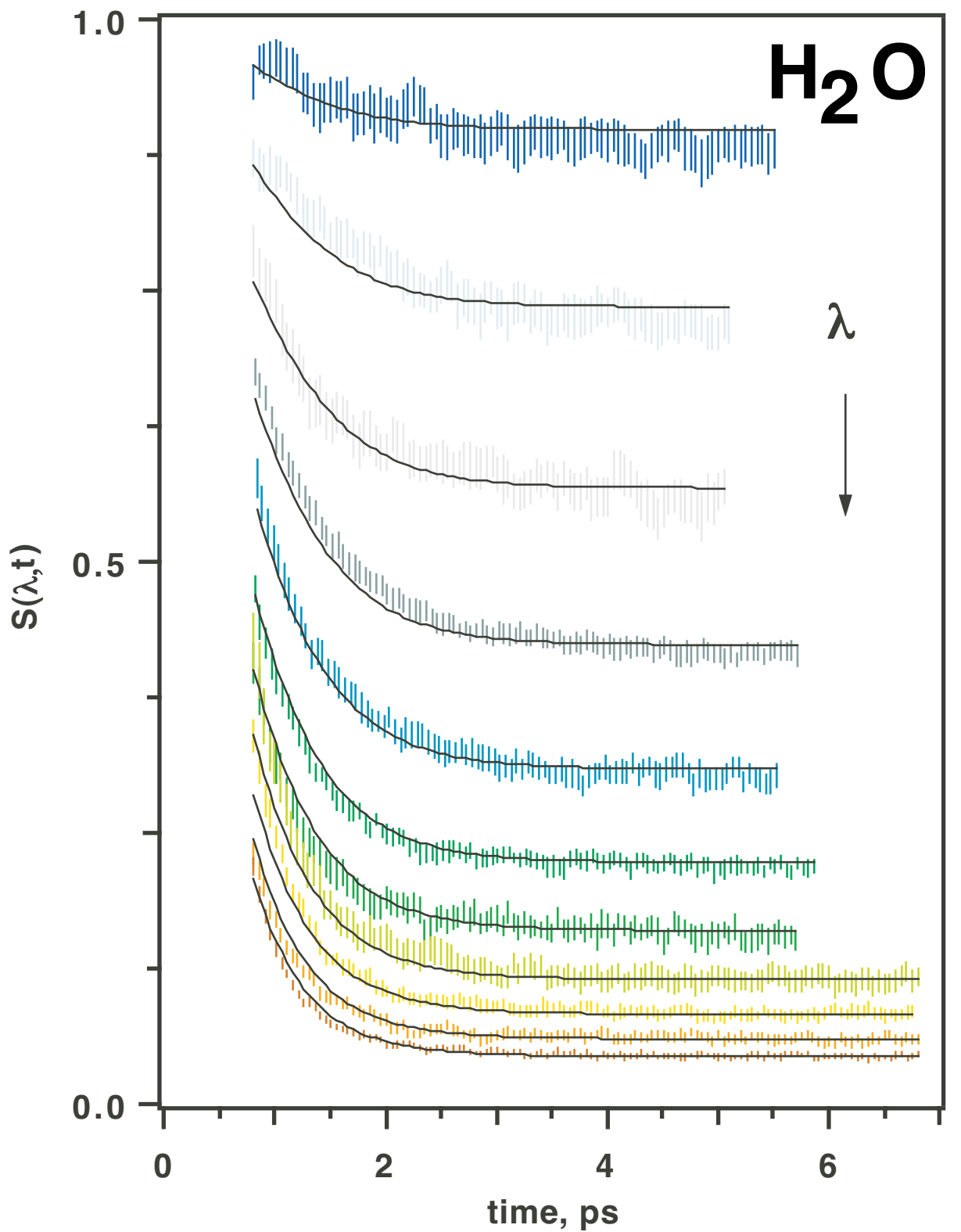
Lian et al., Figure 5



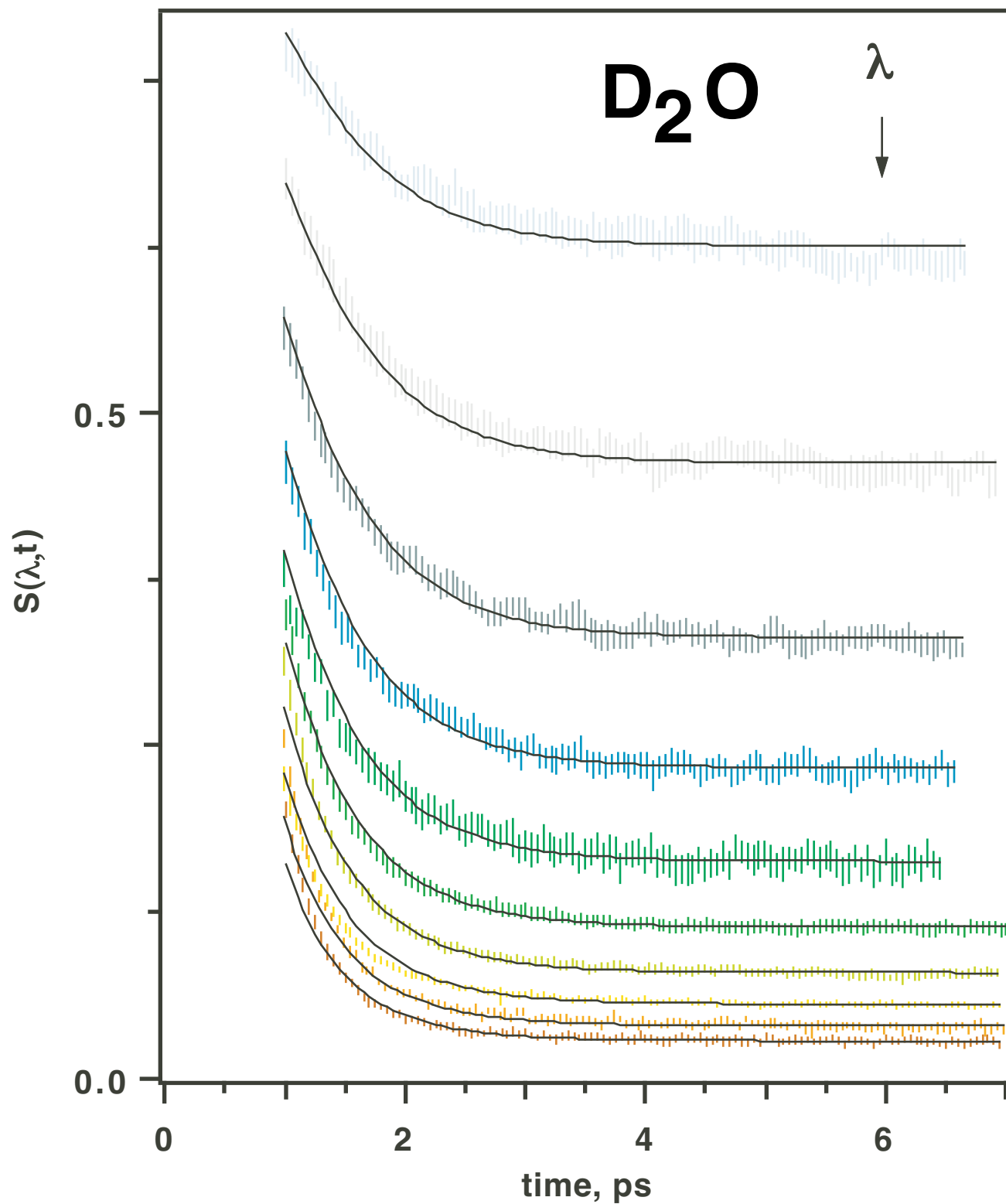
Lian et al., Figure 6



Lian et al., Figure 7



Lian et al., Figure 8



Lian et al., Figure 9

SUPPLEMENTARY MATERIAL**JP*******Journal of Physical Chemistry A, Received *******Supporting Information.****Solvation, relaxation, and geminate recombination of electrons generated by two 200 nm photon ionization of liquid H₂O and D₂O.**

Rui Lian, Robert A. Crowell, and Ilya A. Shkrob.

*Chemistry Division, Argonne National Laboratory, Argonne, IL 60439***Appendix A. The absorption spectrum of hydrated electron.****A.1. Background.**

Although many absorption spectra of hydrated electron in H₂O and D₂O were reported in the literature, there are very few such spectra that exhibit the acceptable S/N ratio in the near IR. Good quality data in this spectral region are needed for the reconstruction of the time-dependent TA spectra of pre-solvated electron using the method discussed in section 2. The prime concern is the accuracy of the Gaussian fit to the low-energy wing of the e_{aq}^- spectrum.

Recently, Bartels and coworkers [1] obtained a large set of spectral data for radiolytically-generated e_{aq}^- at 25–300 °C and fitted this set globally to eqs. (2) and (3) using the temperature-dependent exponent

$$\nu = 1.9488 + 0.0012895t. \quad (\text{A1})$$

where t is the temperature in °C. For H₂O, they obtained

$$E_{\max}(eV) = 1.79 - 0.0025407t + 2.5384 \times 10^{-17}t^5, \quad (\text{A2})$$

$$W_G(eV)/\sqrt{\ln 2} = 0.343 + 0.000290411t + 6.613 \times 10^{-6}t^2 - 4.10413 \times 10^{-8}t^3 + 5.33721 \times 10^{-11}t^4, \quad (\text{A3})$$

and $W_L = 0.51$ eV. For D₂O, the width $W_L = 0.49$ eV and

$$E_{\max}(eV) = 1.84 - 0.00268t + 4.13 \times 10^{-17}t^6, \quad (\text{A4})$$

$$W_G(eV)/\sqrt{\ln 2} = 0.337 + 5.5 \times 10^{-4}t + 2 \times 10^{-8}t^3 - 1.9 \times 10^{-10}t^4 - 3.55 \times 10^{-13}t^5, \quad (\text{A5})$$

To obtain eqs. (A1) to (A5), the e_{aq}^- spectra acquired in steps of 50 nm between 0.3 and 1.7 μm were fit using eqs. (2) and (3) with the floating parameters ν , W_G and E_{\max} using the least squares method; the optimum parameters were then polynominally interpolated.

Figs. 3S(a) and 3S(b) show the temperature dependencies of the parameters ν , W_G , and E_{\max} given by eqs. (A1) to (A5). As seen from the $\nu(t)$ plot given in Fig. 3S(a), the high-energy wing of the electron spectrum ($E > E_{\max}$) is Lorentzian ($\nu \approx 2$) only near the room temperature; e.g., at 300 °C, $\nu \approx 2.35$ and the spectra are much flatter at the top than the room-temperature spectra, for which $\nu \approx 1.95$ (see Fig. 4S). In the previous studies, the shape of the spectrum for $E > E_{\max}$ was assumed to be Lorentzian with a temperature-invariant exponent $\nu = 2$; this assumption is no longer tenable. The variation in the Gaussian width W_G of the half-spectra with increasing temperature is nonnegligible (ca. 20% over the temperature interval of 200 °C), although it is much less than a decrease in E_{\max} (ca. 50% over the temperature interval of 300 °C). It is this relative constancy of the spectral profile vs. the temperature which provides the rationale for the "continuous shift" and "temperature jump" models discussed in sections 1 and 4.2.

The blue side of the electron spectrum ($E > E_{\max}$) is less perfectly approximated by eq. (2) than the red side ($E < E_{\max}$) is approximated by eq. (3), whether a fixed ($\nu = 2$) or variable parameter ν is used (Fig. 3S(a)). While on the red side the absolute deviation of the data points from the Gaussian shape eq. (3) is less than 5-10 %, the deviation on the blue side is typically 5-10 %, depending on the wavelength of the analyzing light. The further into the UV, the worse is the overall fit quality. For this reason, the global least-squares fit is a trade-off: the better is the fit quality for the extension of the spectrum to the near-IR, the worse is the fit quality for the extension of this spectrum to the blue, and vice versa. Hence the uncertainty in the position of the absorption maximum E_{\max} reflected in the scatter of the reported values. Since the electron spectrum is flat at the top, the location of this maximum depends on the exact functional form of the prescribed profile of the spectrum. Inasmuch as this location depends on how well the Lorentzian curve approximates the data points for $E > E_{\max}$, the position of this maximum depends on the extent of the spectrum to the blue. As the quality of the spectral reconstruction given by eq. (1) in section 2 crucially depends on the accuracy of the e_{aq}^- spectrum in the near IR, parameterizations were obtained that are most accurate in that particular spectral region. This feat can only be achieved by truncating the e_{aq}^- spectrum in the blue at 400 nm.

A.2. Electron spectrum from flash photolysis data.

To obtain a good-quality spectrum of e_{aq}^- , hydrated electrons were generated by 248 nm (one-) photon excitation of 330 μm ferrocyanide (hexacyanoferrate (II)) and 4.8 mM sulfite using 15 ns FWHM, 10 mJ pulses from an ArF excimer laser (Lambda Physik model LPX120i) in a 1.36 mm optical path cell with suprasil windows. These two aqueous anions photoreact according to



and



The anion absorptivities and the quantum yields for electron photodetachment are 4270 M⁻¹ cm⁻¹ and 0.674 for ferrocyanide and 50 M⁻¹ cm⁻¹ and 0.108 for sulfite, respectively. The advantage of using ferrocyanide is the high electron yield; the disadvantage is that ferricyanide anion (hexacyanoferrate (III)) generated in rxn. (A6) absorbs light at $\lambda < 450$ nm. Thus, to obtain the electron spectrum in the blue, electron photodetachment from sulfite should be used (the SO_3^- radical generated in rxn. (A9) does not absorb > 400 nm).

The 248 nm beam uniformly illuminated a rectangular 3 mm x 6 mm aperture placed onto the front window of the photocell. This beam was normal to the window. The analyzing light from a pulsed 75 W Xe lamp was crossed at 30° with this excitation beam. After traversing the sample, the analyzing light passed through an appropriate cutoff filter and was focussed on the photodiode using a 7 cm focal length achromat. The wavelength of the analyzing light was selected using the same narrowband interference filters used in our pump-probe kinetic studies. The signal from the fast Si and Ge photodiodes (of the same type as in section 2) loaded into 50 Ω was amplified using a 1.2 GHz video amplifier (Comlinear model CLC449) and sampled by a digital signal analyzer (Tektronix model DSA601). The response time of this detection system was 3 ns. Two energy meters (Molelectron model J25-080) were used to measure the power of the incident and transmitted UV light. 0.2-1 L of aqueous N₂-saturated solution of K₄Fe(CN)₆ or Na₂SO₄ (99.99+% ultrapure grade, Aldrich) was circulated through the cell using a peristaltic pump. The typical flow rate was 2-3 ml/min; the repetition rate of the laser was 1 Hz. All measurements were carried out at 24 °C. Each kinetic trace was an average of 20-30 laser shots. The time profile of these kinetic traces (for wavelengths λ where only electron absorbed) was independent of λ ; no effect of continuous exposure of the sample to the UV light was observed. The half time of the electron decay was 400 ns for ferrocyanide and 5 μs for sulfite, respectively. The life time of e_{aq}^- was controlled by the homogeneous recombination in the bulk; for sulfite, a slow scavenging reaction with an impurity (likely, traces of oxygen) was also significant. The time-dependent TA signal was integrated between 50 and 120 ns and these integrals (normalized by the integral at 700 nm) were plotted vs. λ and fit using eqs. (2) and (3) with $\nu = 2$.

The composite spectrum of e_{aq}^- in H₂O is shown in Fig. 5S. For $\lambda < 500$ nm, the data for sulfite and ferrocyanide photolysis are both shown; at higher photon energy, only sulfite data are shown. The optimum fit parameters obtained for this data set are $E_{max} = 1.699 \pm 0.005$ eV, $W_G = 0.422 \pm 0.005$ eV, and $W_L = 0.492 \pm 0.007$ eV (the standard deviations are given). The data for D₂O (only low-energy "tail" of the spectrum is shown in Fig. 6S) can be fit using the same W_L and W_G and $E_{max} = 1.749$ eV (which is ca. 3%

higher than the light water estimate). As shown in Figs. 5S and 6S, all residuals are less than 0.02. For $\lambda < 500$ nm, our data for e_{aq}^- in H₂O compare well with the data given by Jou and Freeman [1] (see Table 2S), although the fit parameters are different. Ironically, using the "optimum" parameters given by Jou and Freeman makes the fit quality in the near-IR worse, because their parameters were, apparently, optimized to provide the best fit for the visible and UV regions. The same applies to the parameterization of the e_{aq}^- spectrum by Bartels and coworkers [2]: As shown in Table 2S and Fig. 5S, the $S(E)$ curve calculated using the spectral parameters given by eqs. (A1) to (A5) fits well the experimental data on the blue side of the spectrum but much worse on the red side of the spectrum. On the red side, $S(E)$ is systematically underestimated by as much as 5%.

Since the reconstruction of the absorption spectrum of pre-thermalized electron by the method discussed in section 2 critically depends on the quality of the e_{aq}^- spectrum in the near IR (where e_{aq}^- absorbs poorly), the parameterization given above is preferable to that given by others. Given that in the near IR, the ratio of the TA signal in the "spike" to the TA signal from the thermalized electron at $t=5$ ps can be as large as 20:1 (Fig. 4), even a small error (1-2%) in the e_{aq}^- spectrum $S(\lambda)$ used for the normalization translates into a 10-50% error in the amplitude of $S(\lambda, t)$ at short delay time. These large error bars undermine the confidence in the spectral data obtained using the normalization method on a very short time scale. Other reasons for treating such data with caution, *viz.* the thermal effects and wavelength dependence of the probe characteristics, are briefly discussed in sections 2 and 3 in the text.

While there are several alternatives to the (obviously, imperfect) normalization method used in this work, these methods proved to be equally problematic for obtaining a good-quality sub-picosecond TA spectrum over a sufficiently wide wavelength range. Scanning the wavelength of the probe light for a fixed delay time, by using a set of interference filters or a monochromator (as done to generate the spectrum shown in Fig. 13S), does not correct for the wavelength-dependent change in the width (chirp) in the probe pulse and the group velocity mismatch. [3] Obtaining two-dimensional TA data using diode array or CCD detectors makes it possible to track these changes better, [4] but the dynamic range of these detectors is small, and it is impossible to cover a large section of the e_{aq}^- spectrum in the near-IR, where the intensity of transmitted light decreases precipitously with the increasing wavelength. Using optical parametric amplifiers instead of the white-light supercontinuum generation leads to the same difficulties when λ is changed over a sufficiently wide range, especially in the near- and mid- IR. [5] Since the pulse characteristics continuously change with the probe wavelength, it is impossible to interpret the data without prescribing an *ad hoc* kinetic model, and this makes the resulting TA spectra dependent on the details of such a model. Our goal was to eliminate such a dependency, hence our reliance on the normalization method.

Appendix B. Instruction for the retrieval of kinetic data from the supplied ascii file.

Included in this Supplement is a 288Kb-long ASCII file named **H2O_D2O_traces.txt** containing the kinetic traces for light and heavy water. These kinetics were sampled with a time step of 50 fs out to 5-7 ps. We also have a nearly complete set of such kinetics sampled with a step of 500 fs out to 25 ps. The data are formatted as an Igor text wave (suitable for Igor 4.0). It is simple to read these data using other graphics packages. Each kinetic trace is tagged by its `<id>` label which consists of the wavelength λ in nanometers and identifier "H" (for H₂O) or "D" (D₂O) at the end (e.g., `t1150H` is the array of delay times for the electron in light water). The three columns for each section of the record (that starts with **BEGIN** and ends with **END**) that corresponds to a given wavelength are

- t<id>:** delay time t in picoseconds
- od<id>:** photoinduced optical density $S(\lambda, t)$ (see section 2).
- dod<id>:** $\pm 95\%$ confidence limits for the quantity above.

The format of the data file is

```

IGOR
WAVES/D  t<id1> od<id1>      dod<id1>
BEGIN
<time  $t$ , ps>  <normalized  $S(\lambda, t)$ > < $\pm 95\%$  confidence limits>
...
END
X SetScale/P x 0,1,"", t<id1>; SetScale y 0,0,"", t<id1>
X SetScale/P x 0,1,"", od<id1>; SetScale y 0,0,"", od<id1>
X SetScale/P x 0,1,"", dod<id1>; SetScale y 0,0,"", dod<id1>

WAVES/D  t<id2> od<id2>dod<id2>
BEGIN
...
END
X SetScale/P x 0,1,"", t<id2>; SetScale y 0,0,"", t<id2>
X SetScale/P x 0,1,"", od<id2>; SetScale y 0,0,"", od<id2>
X SetScale/P x 0,1,"", dod<id2>; SetScale y 0,0,"", dod<id2>

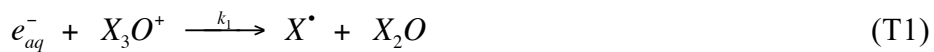
.....
etc.

```

For further instruction, contact IAS at shkrob@anl.gov.

Table 1S.

Simulation parameters for IRT modeling of recombination dynamics (X=H,D) of hydrated electron in the room-temperature liquid water (after refs. [1])



parameter	H ₂ O	D ₂ O
diffusion coefficients, x10 ⁻⁵ cm ² /s		
<i>e</i> _{aq} ⁻	4.9	3.9
<i>X</i> ₃ <i>O</i> ⁺	9.0	6.7
<i>XO</i>	2.8	2.2
reaction constants, etc. ^{a)}		
<i>k</i> ₁ , x10 ¹⁰ M ⁻¹ s ⁻¹	2.3	1.0
<i>k</i> ₂ , x10 ¹⁰ M ⁻¹ s ⁻¹	3.1	2.5
reaction velocity <i>v</i> (rxn. (T1)), m/s	4.0	1.5
other parameters ^{b)}		
<i>σ_G</i> , nm ^{c)}	2.4	2.1

a) Reaction radii of 0.5 and 0.54 nm were assumed for rxns. (T1) and (T2), respectively.

b) Dielectric constant of 78 and initial *X*₃*O*⁺...*OX* distance of 0.28 nm were assumed for both liquids.

c) The width of the *r*²-Gaussian electron distribution.

Table 2S.**A comparison between the normalized spectra of hydrated electron in H₂O at 24°C.**

$\lambda, \mu\text{m}$	this work	Bartels et al. [1] ^{b)}	Jou & Freeman [2]
0.5	0.290	0.32	0.293
0.6	0.656	0.699	0.647
0.7 ^{a)}	1	1	1
0.8	0.902	0.841	0.871
0.9	0.572	0.502	0.57
1.0	0.313	0.261	0.295
1.1	0.163	0.13	0.148
1.2	0.085	0.066	0.082
1.3	0.045	0.034	0.042
1.35	0.033	0.025	0.033
1.4	0.025	0.018	0.024

a) the spectra were normalized at this wavelength.

b) calculated using eqs. (2), (3) and (A1) to (A3).

Figure captions.

Fig. 1S

Time profiles of normalized photoinduced TA signals (ΔOD_λ) from a 1.4 μm thick film of amorphous hydrogenated silicon alloy (8 at % H) grown by the CVD deposition from $\text{SiCl}_4/\text{Ar}/\text{H}_2$ plasma on a 1 mm thick suprasil substrate (this sample was obtained from Prof. H. Fritzsche at the James Frank Institute, U. of Chicago). Kinetic traces obtained at four different wavelengths λ are shown (as indicated in the plot). The TA signal at the maximum linearly scales with the 200 nm photon fluence. The vertical bars are 95% confidence limits; the solid lines are simulations (a Gaussian response function convoluted with biexponential decay to a plateau). The sample was inserted in such a way that the plane of the film corresponded to that of the jet surface. Similar kinetics were obtained for each probe wavelength and used to determine the response function of the setup and the origin of time (i.e., the center of the Gaussian excitation pulse).

Fig. 2S

(a) The dependence of the TA signal ($\lambda=800$ nm) from hydrated electron in liquid H_2O at 25 °C (observed at $t=10$ ps after the photoionization) as a function of the power of 200 nm pulse. For this measurement, the pump and probe beams were tightly focussed. Note the double logarithmic scale. The initial slope of 1.84 ± 0.07 is consistent with biphotonic ionization of water by 200 nm light. (b) Normalized TA kinetics at the extremes of the dynamic range shown in (a). The traces were normalized at $t=5$ ps. Trace (i) was obtained for the highest pump power; trace (ii) was obtained for the lowest pump power in (a). The solid lines are guides to the eye. Note the logarithmic time scale and non-zero origin of the vertical axis. The rapid decay on subnanosecond time scale is due to the cross-recombination in the water bulk.

Fig. 3S

Temperature dependencies of (a) the parameter ν (eq. (A1)) and (b) the energy of the band maximum E_{\max} (to the left; eqs. (A2) and (A4)) and Gaussian half-width $W_G/\sqrt{\ln 2}$ (to the right; eqs. (A3) and (A5)) for hydrated electron in liquid H_2O (solid lines) and D_2O (dashed lines). See **Appendix A** for more detail.

Fig. 4S

Simulated absorption spectra $S(E)$ of hydrated electron (plotted vs. the photon energy E) in light (solid lines) and heavy (dashed lines) liquid water at (i) 25 °C and (ii) 200 °C. Eqs. (2) and (3) with the parameters given by eqs. (A1) to (A5) were used to simulate these spectra. The spectra for D_2O were shifted to the red by 38.5 meV at both of these temperatures. The spectra are normalized at $E = E_{\max}$. At the higher temperature, the spectrum is flatter at the top.

Fig. 5S

Vide infra: Normalized TA signal from the hydrated electron generated by 248 nm laser photolysis of ferrocyanide (*filled circles*) and sulfite (*open squares*) in the room-temperature liquid H₂O. See [section A.2 in Appendix A](#) for more detail. Pink circles indicate that data obtained using a Ge photodiode detector, red circles are for the data obtained using a Si photodiode. The red line is the least-squares fit to eqs. (2) and (3) with $\nu = 2$ (see [section A.2](#) for the optimum parameters). Green line gives the simulated spectrum obtained using the parameters given by eqs. (A1) to (A5). *Vide supra:* the residuals (*same color coding*).

Fig. 6S

Same as [Fig. 5S](#), for hydrated electron in D₂O (ferrocyanide data only). The open squares and open circles stand for the data obtained Ge and Si detectors, respectively. The solid line is the fit obtained as explained in [section A.2 of Appendix A](#).

Fig. 7S

The effect of addition of 1 M perchloric acid to water on the decay kinetics of hydrated electron in liquid room-temperature H₂O. TA signal obtained for the probe wavelength of 1.3 μ m is shown in the acidic solution (*open squares*) and neat water (*open circles*). The initial "spike" from pre-solvated electron is not shown; the kinetic traces were normalized at $t=5$ ps. The vertical bars are 95% confidence limits for each data point. The Gaussian radii of the 200 nm pump and 1300 nm probe beams were 37 μ m and 14 μ m, respectively. The kinetic traces indicated by the symbols were obtained using 2.3 μ J excitation pulse, the traces indicated by slim vertical bars with caps were obtained at lower power, 1.3 μ J. The two series of data match well, suggesting inefficient cross recombination. The solid line is the exponential function that corresponds to the time constant of 43 ps which is close to the life time of hydrated electron that undergoes reaction with H₃O⁺ in the bulk ($k = 2.3 \times 10^{10}$ M⁻¹ s⁻¹, see [Table 1S](#)). These kinetic data suggest that at least 90-95% of the ΔOD_{1300} signal at $t>5$ ps is from the hydrated electron.

Fig. 8S

The spectral data of (a) [Fig. 5\(a\)](#) and (b) [Fig. 6\(a\)](#) replotted as a function of the photon energy E of the probe light.

Fig. 9S

Expanded section of [Fig. 8](#) (the same color coding as in [Fig. 8](#)).

Fig. 10S

Expanded section of [Fig. 9](#) (the same color coding as in [Fig. 9](#)).

Fig. 11S

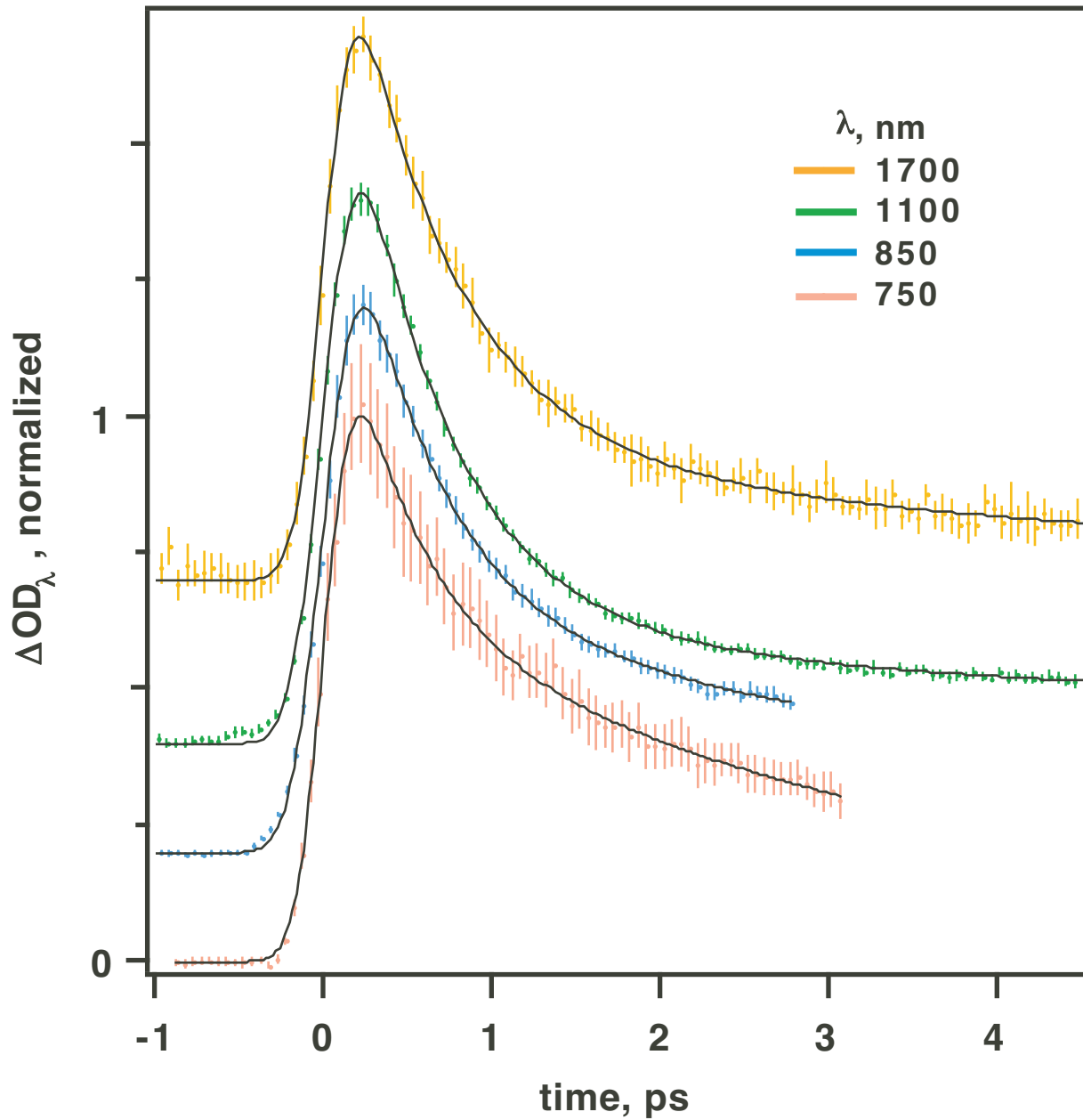
TA spectra for the electron in D₂O analyzed using eqs. (2) and (3) with the variable parameter ν and fixed parameter W_L (i.e., in the same way as the high-temperature spectra analyzed by Bartels et al. [1] and discussed in section A.1 of Appendix A, eqs. (A1) to (A5)). See section 4.2 for more detail. The time windows are given in the color scale to the right of the plot. The vertical bars are 95% confidence limits. The solid lines are least-square fits; the dashed lines are guides to the eye. The bold solid (yellow) line is the spectrum $S(E)$ of hydrated electron in D₂O. The time dependence of the optimum parameters is given in Fig. 12S.

Fig. 12S

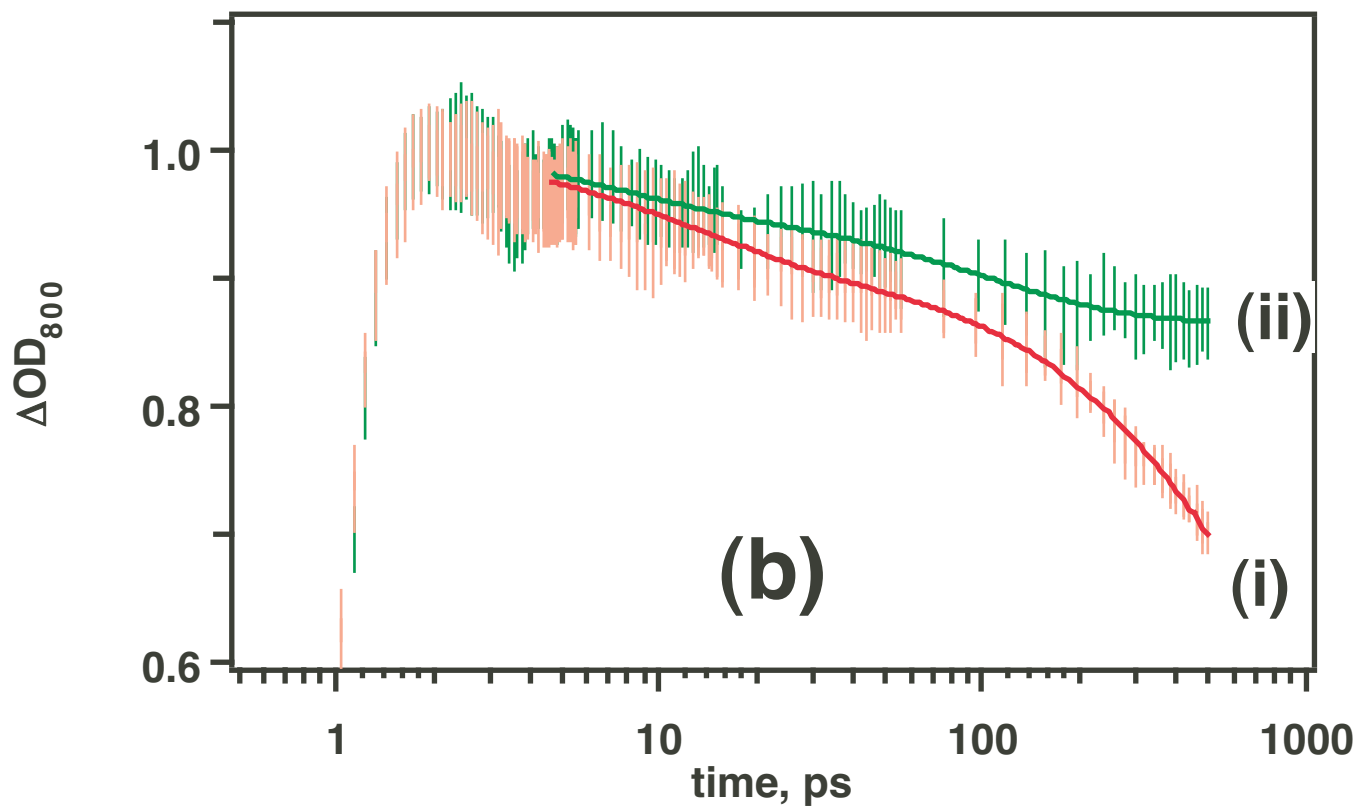
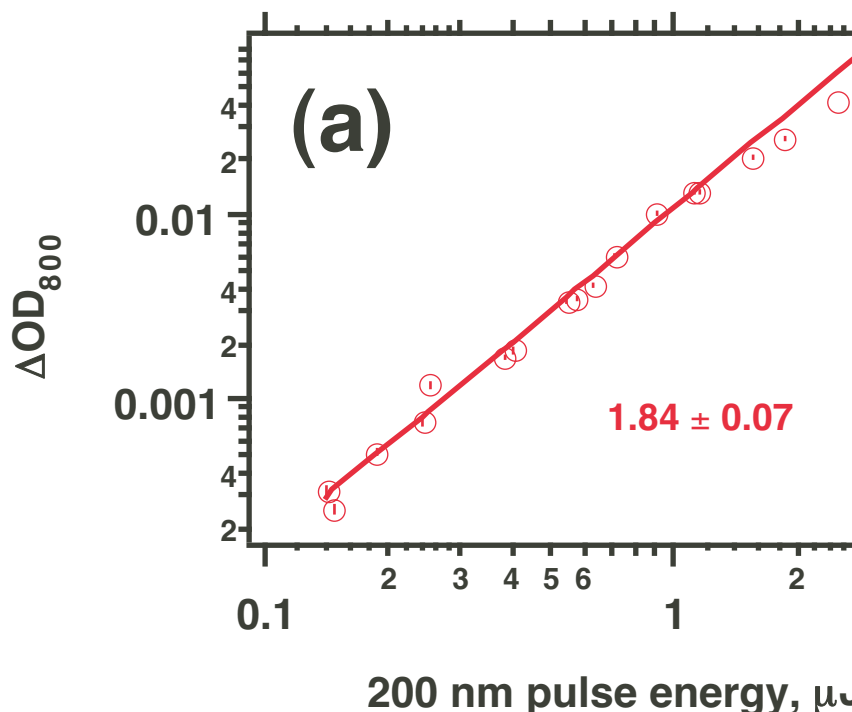
Time profiles of the optimum parameters (a) E_{\max} , (b) W_G , and (c) ν for the electron in D₂O. See section 4.2 and Fig. 11S for more detail.

Fig. 13S

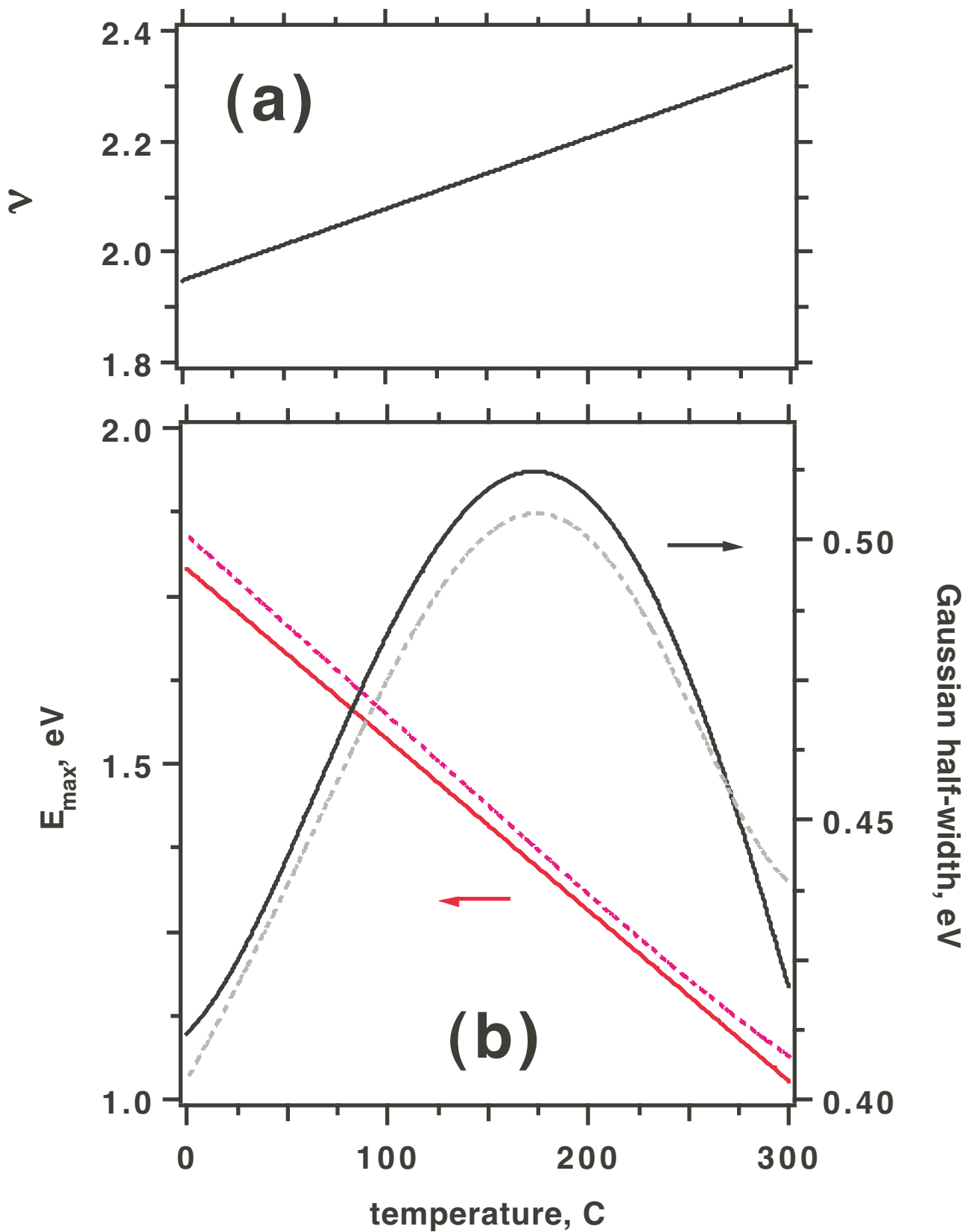
Open circles: TA signal for the electron in D₂O vs. the wavelength λ of the probe light ($\lambda > 1.1 \mu\text{m}$). The delay time between the 200 nm pump and the probe pulses was fixed (this delay time corresponded to the last 10% of the pump pulse duration). The data were obtained in a single take; a set of interference filters on a rotating wheel was used to select the probe wavelength from the white light supercontinuum. The solid line is a guide to the eye.



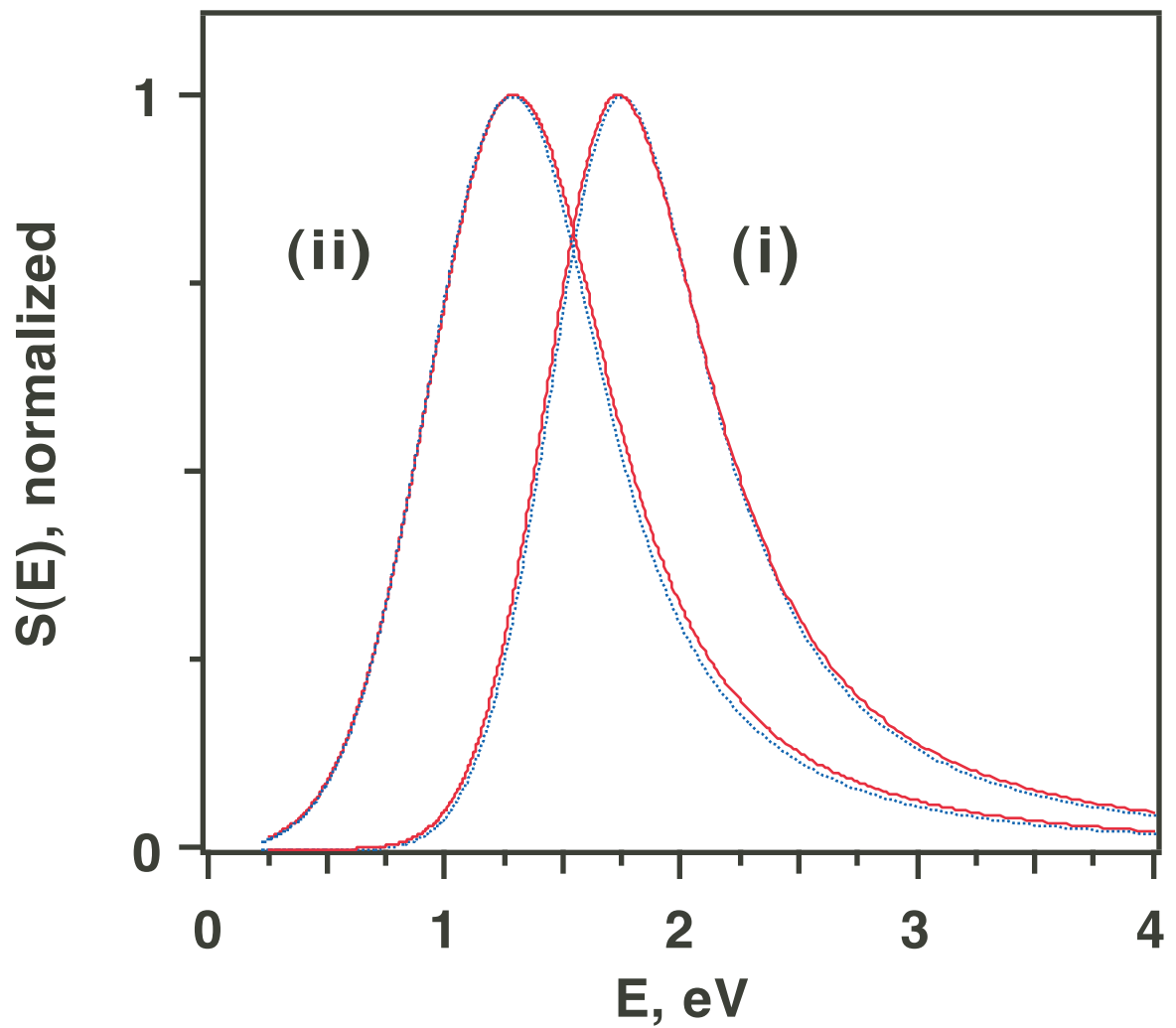
Lian et al., Figure 1S



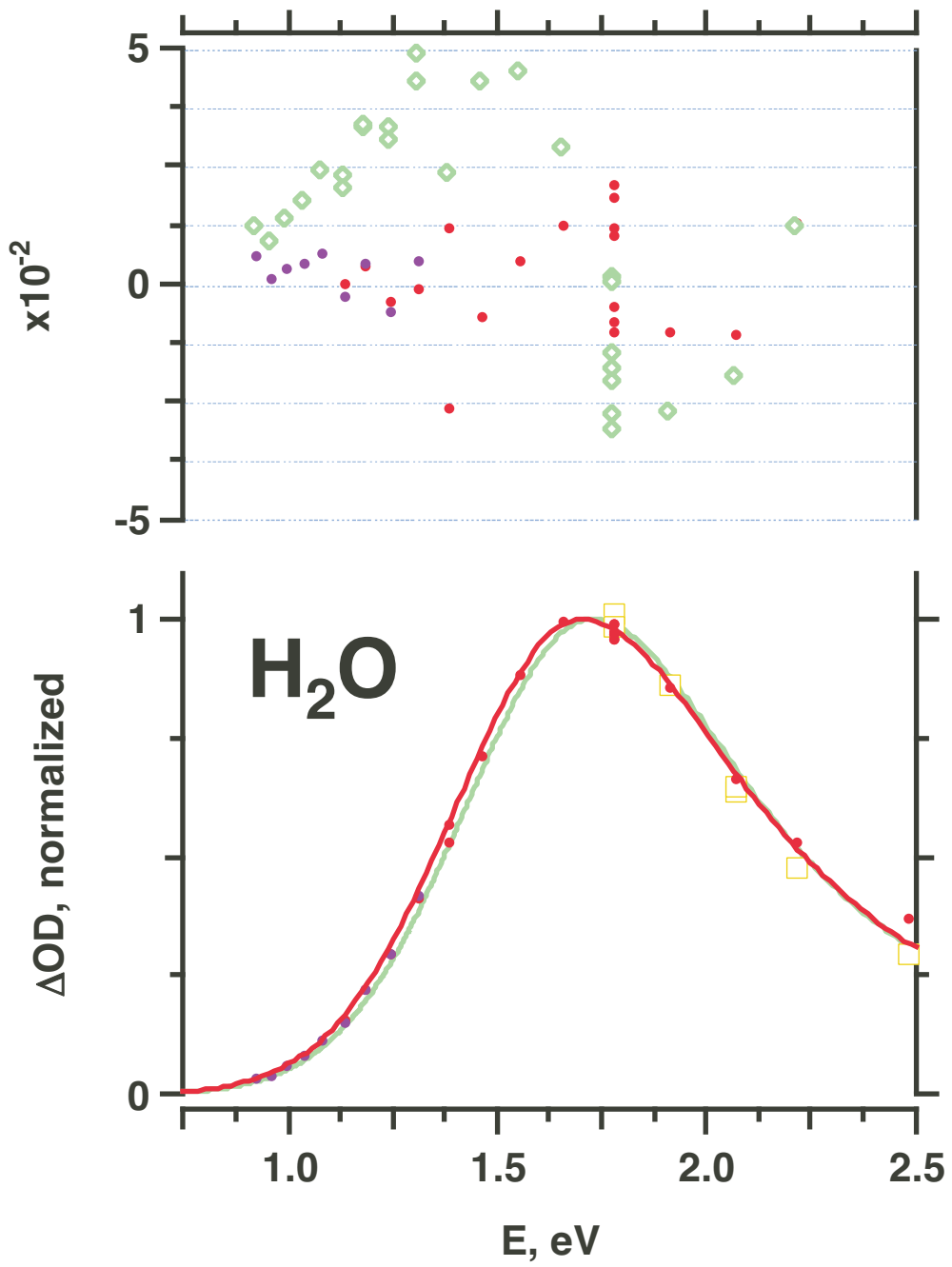
Lian et al., Figure 2S



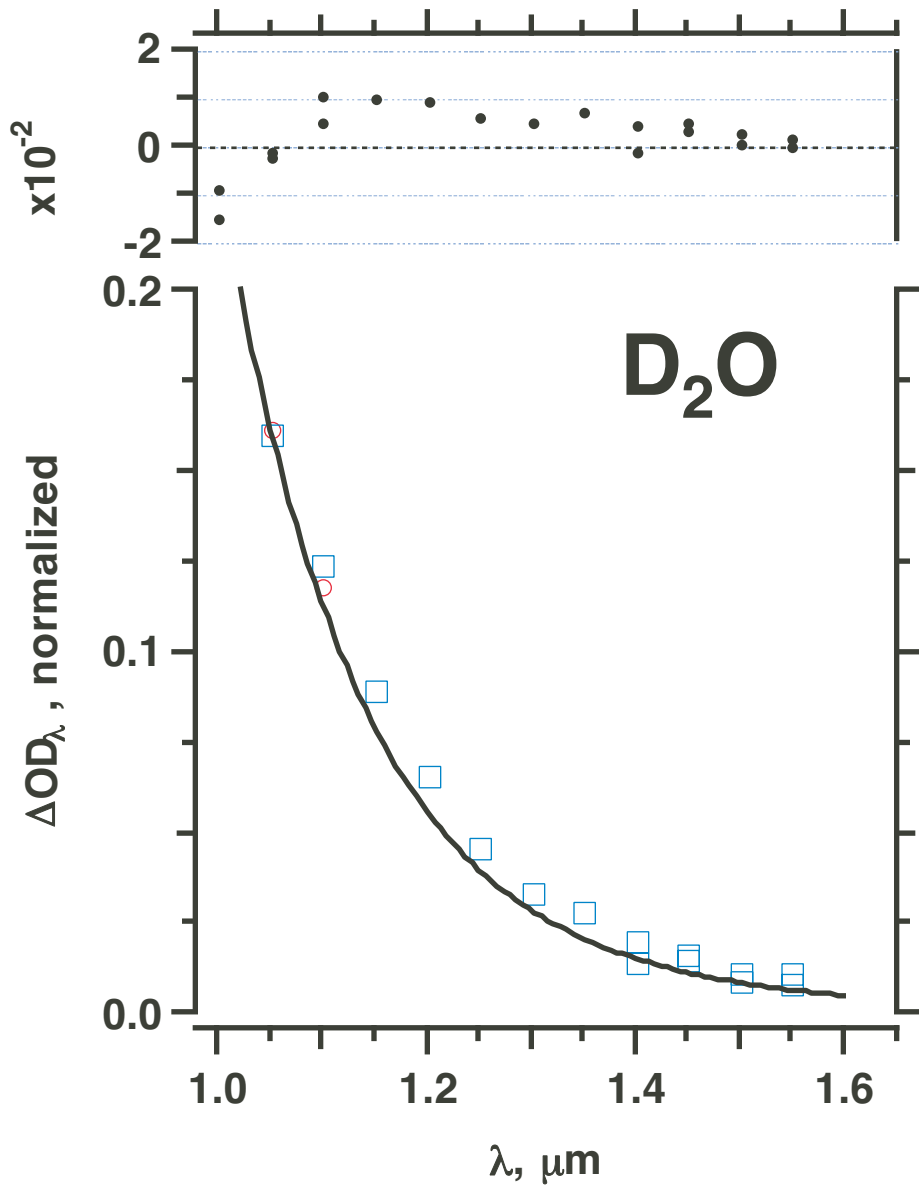
Lian et al., Figure 3S



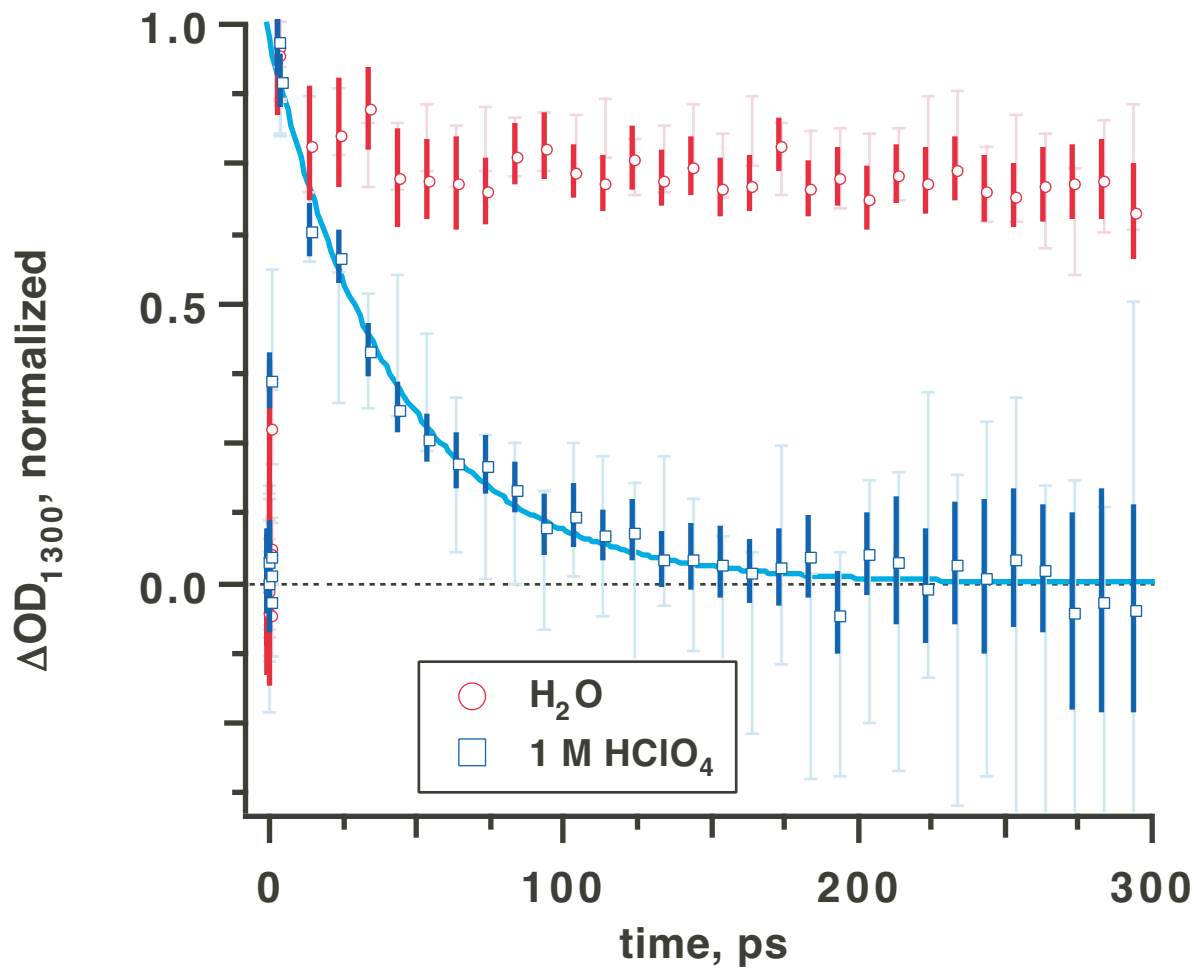
Lian et al., Figure 4S



Lian et al., Figure 5S

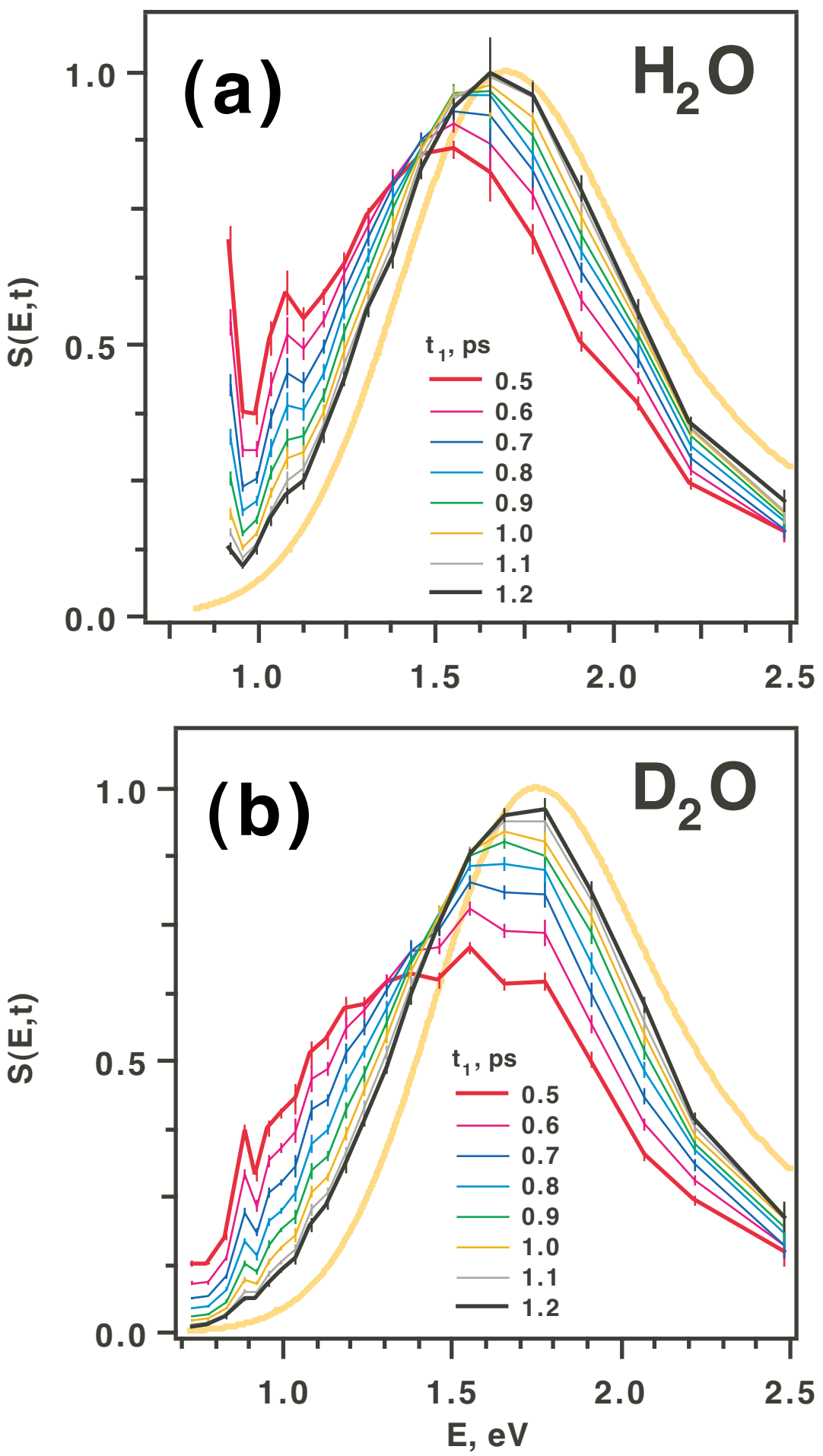


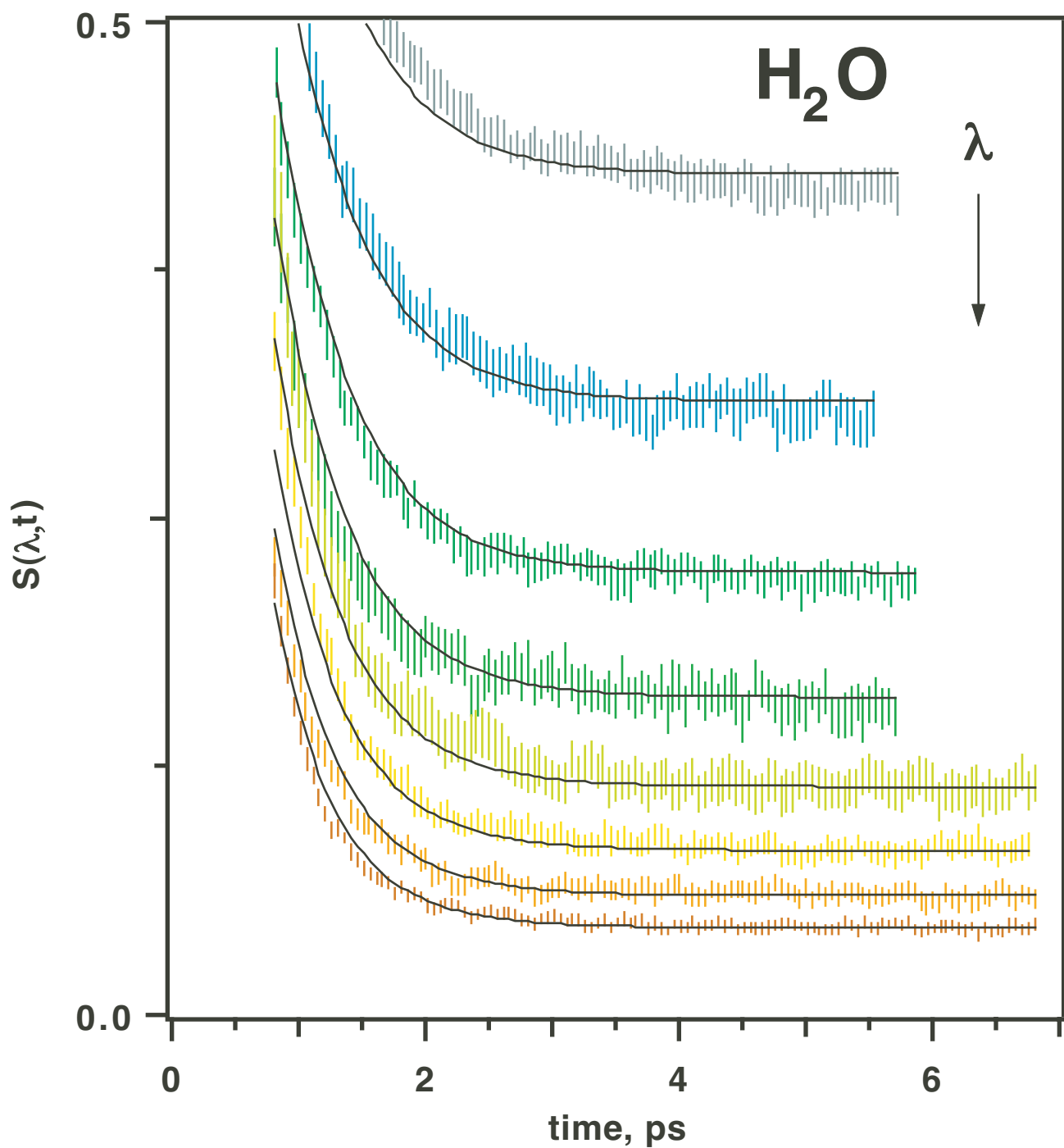
Lian et al., Figure 6S



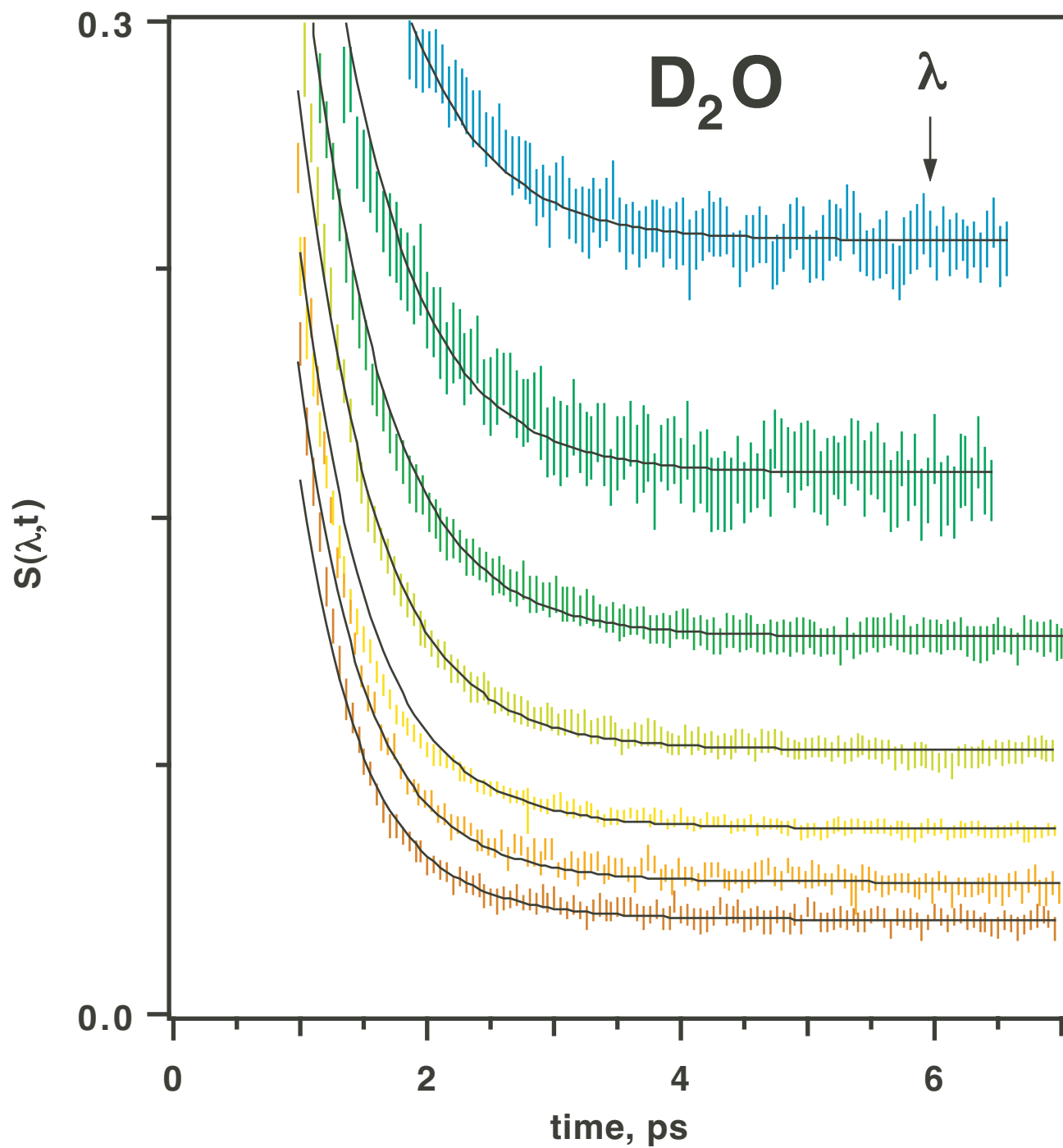
Lian et al., Figure 7S

Lian et al., Figure 8S



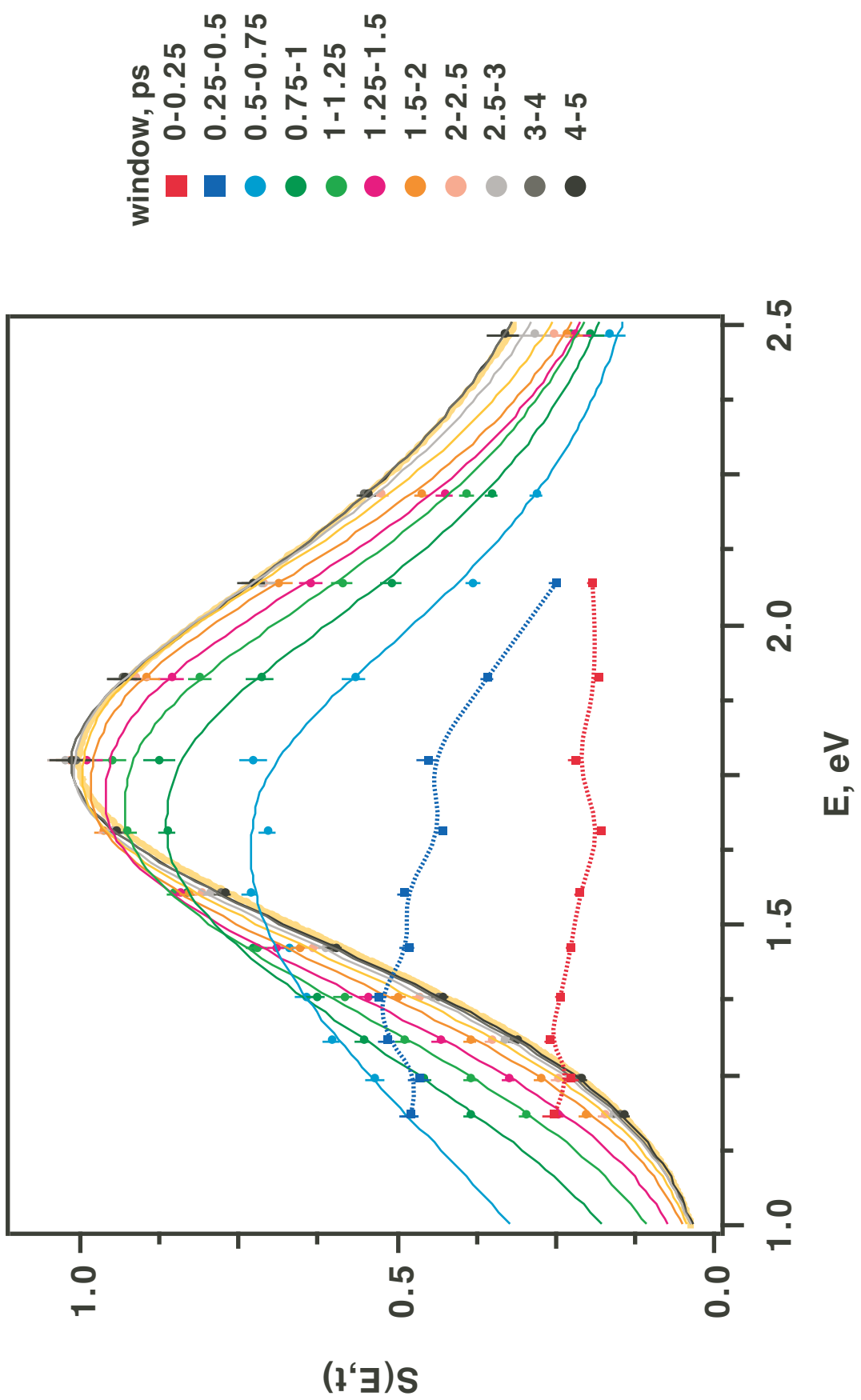


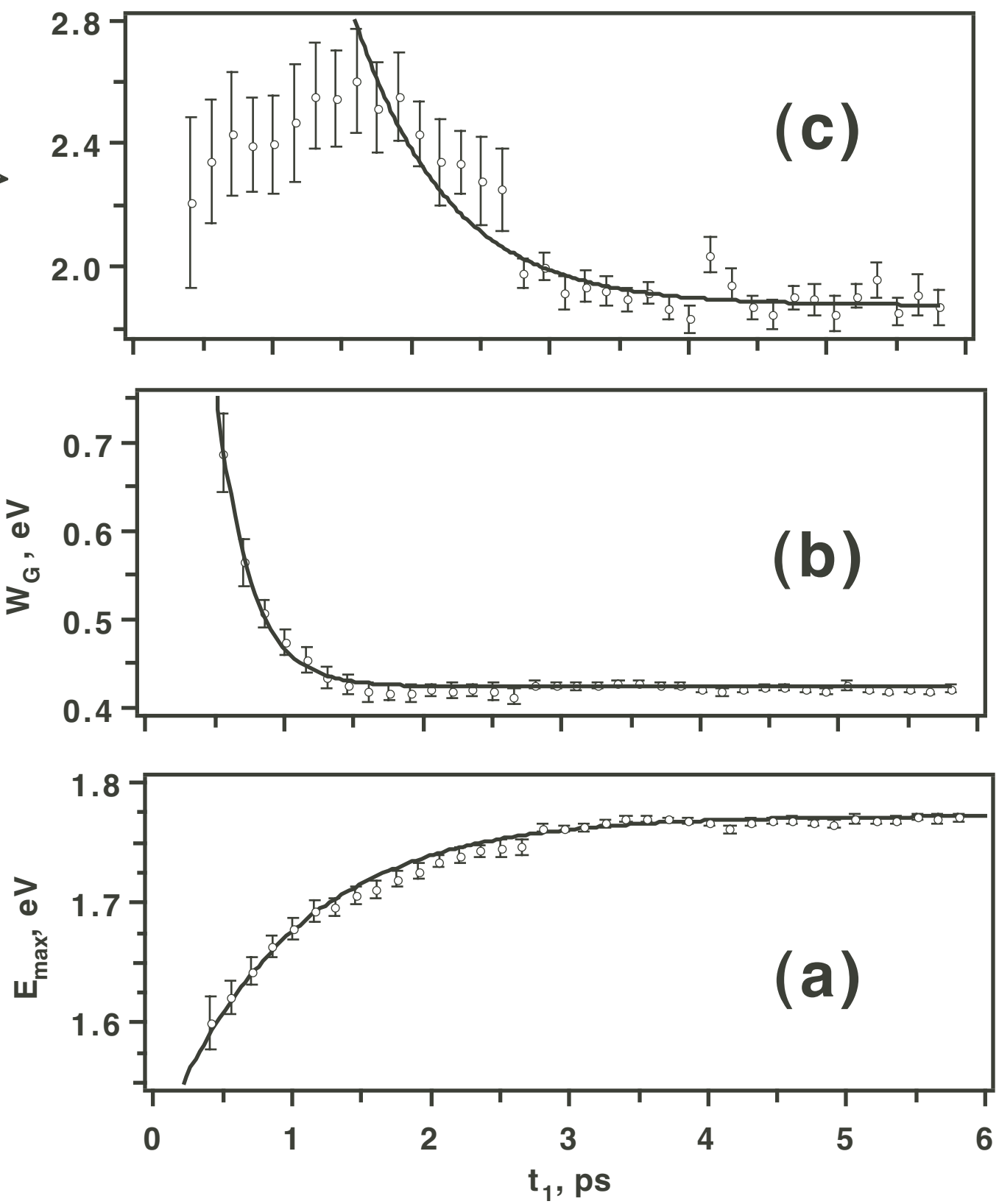
Lian et al., Figure 9S



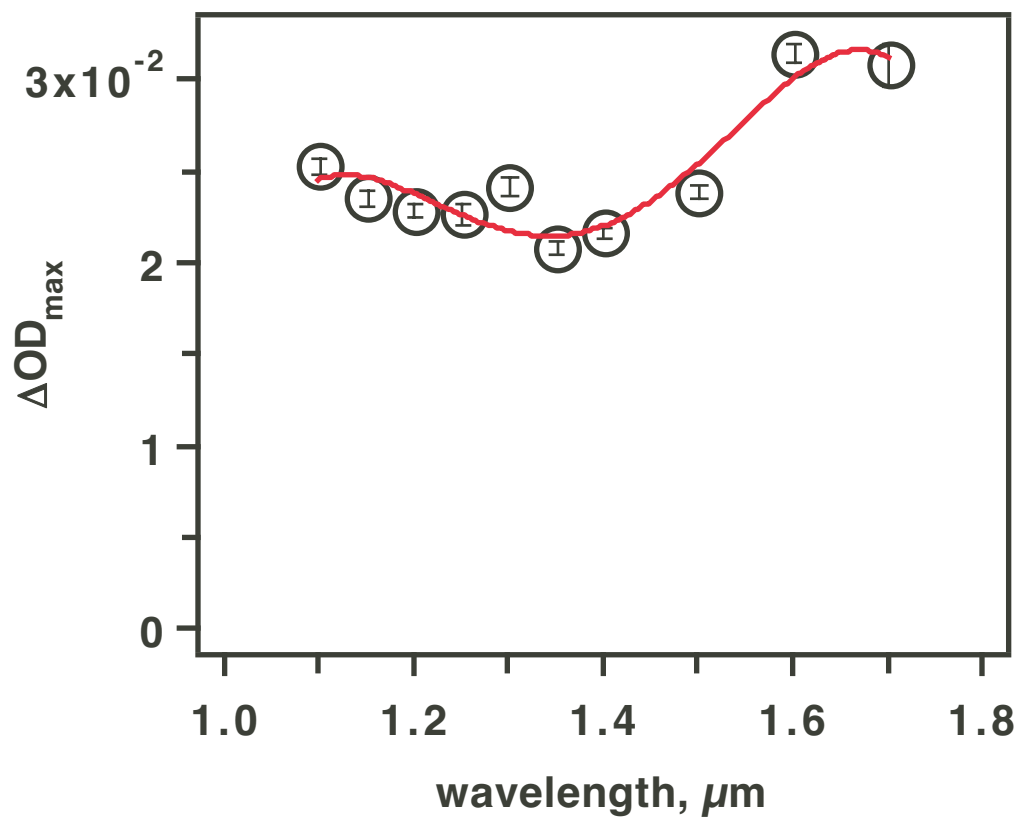
Lian et al., Figure 10S

Lian et al., Figure 11S





Lian et al., Figure 12S



Lian et al., Figure 13S